Bioinspired Mo, W and V complexes bearing a highly hydroxyl-functionalized Schiff base ligand

Pasi Salonen[a], Anssi Peuronen[a,b], Ari Lehtonen[a,*]

* Corresponding author
[a] Group of Inorganic Materials Chemistry, Department of Chemistry, University of Turku, FI-20014 Turku, Finland.
[b] Laboratory of Inorganic Chemistry, Department of Chemistry, University of Jyväskylä, FI-40014 Jyväskylä, Finland.

Abstract

A series of bioinspired dioxidomolybdenum(VI), dioxidotungsten(VI) and oxidovanadium(V) complexes $[MoO_2(H_2L^{Saltris})]$, $[WO_2(H_2L^{Saltris})]$ and $[VO(HL^{Saltris})]_2$ were prepared by the reaction of a hydroxyl-rich Schiff base proligand *N*-(1,3-dihydroxy-2-(hydroxymethyl)propan-2-yl)-3,5-di-*tert*-butylsalicylaldimine ($H_4L^{Saltris}$) with metal precursors in methanol solutions. Molybdenum and tungsten complexes crystallize as mononuclear molecules, whereas the vanadium complex forms dinuclear units. From the complexes, $[VO(HL^{Saltris})]_2$ shows activity in the oxidation of 4-*tert*-butylcatechol and 3,5-di-*tert*-butylcatechol, mimicking the action of the dicopper enzyme catechol oxidase.*

Introduction

The easy exploitation of aerial dioxygen in the context of oxidation catalysis represents one of the most desired goals in synthetic organic chemistry because of its ready availability, low cost and environmental compatibility.[1] Nature has perfected the use of the relatively inert dioxygen molecule in a wide variety of metabolic oxidation reactions through metalloenzymes. Efforts to mimic various metalloenzyme active sites by (bio)inorganic chemists can be divided into biomimetic (structural) and bioinspired (functional) modelling.[2,3] A central idea in coordination chemistry is to use ligands with diverse electronic and steric features to modulate the properties of central metals in various model complexes, and thus achieve some properties related to natural enzyme active sites.

The enzymes from the molybdenum oxotransferase superfamily catalyze oxygen atom transfer (OAT) reactions, whereby an oxygen atom is transferred from a high-valent, catalytically active (di)oxidomolybdenum species to a suitable donor/acceptor molecule.[4,5] The superfamily can be divided into three subfamilies, namely xanthine oxidase, sulfite oxidase and DMSO reductase.[6] The active sites of the eponymous enzymes DMSO reductase and sulfite oxidase consist of a monooxido- and dioxidomolybdenum(VI) centers, respectively.[6] They, together with many other molybdoenzymes

List of abbreviations: 3,5-DTBC (3,5-di-*tert*-butylcatechol), 3,5-DTBSQ (3,5-di-*tert*-butylsemiquinone), 3,5-DTBQ (3,5-di-*tert*-butyl-1,2-benzoquinone), 4-TBC (4-*tert*-butylcatechol), 4-TBQ (4-*tert*-butyl-1,2-benzoquinone), OAT (oxygen atom transfer).

have been structurally and functionally modelled by a number of monooxido- and dioxidomolybdenum(VI)- and tungsten(VI) complexes, which find applications in OAT catalysis research.[7]

Vanadates and other vanadium-containing compounds have been studied for decades due to their biological relevance and catalytic activity in a variety of oxidation reactions.[8–11] Especially, the bioinorganic chemistry of vanadium, highlighted by the three vanadium haloperoxidases and V-nitrogenase, as well as the anti-diabetic effects of many vanadium compounds have motivated synthetic chemists to prepare model compounds for use in oxidation catalysis, as well as in structural studies, and in medicinal research.[12–14] Catechol oxidase is an dioxygen-activating dicopper enzyme[15–17] which catalyzes the oxidation of catechols to the corresponding *o*-benzoquinones, producing water as a by-product. A number of vanadium(IV) and vanadium(V) complexes have also been discovered to efficiently catalyze the same reaction.[18–23]

Although compounds that display catechol oxidase mimetic activities are usually reserved for of Cu coordination model compounds[24,25], recently many other metals *e.g.* Co, Mn, Fe, Ni and Zn, as substitutes for copper, have also been used to reach moderate to high conversions of various catechols to *o*-benzoquinones.[26–28] There are also some examples on the catechol oxidase mimicking activity of molecular vanadium(IV) and vanadium(V) complexes.[18–23] It is well established that various catechols readily form redox non-innocent complexes with vanadium, where the vanadium center may be assigned +III, +IV and +V oxidation states.[29–33] There are also some reports for catecholate-containing molybdenum and even tungsten complexes.[34] In the case of vanadium(V) complexation of catechols may lead to a reduction in the metal center (V(V) → V(IV)), sometimes accompanied by cleavage of the oxido ligand.[30,31,33]

The mechanism(s) of vanadium-catalyzed oxidation of catechols are still not fully understood. For example, many vanadium systems apparently demonstrate catechol oxidase- and catechol dioxygenase-like activities simultaneously, leading to a number of oxidation products ranging from intra- and extradiol cleavage products to autoxidation products.[35,36] Furthermore, there is no definitive consensus on the nature of the active catalyst, with some proponents in support of a "common catalyst hypothesis", which states that a specific vanadium-containing, catalytically active species is always formed *in-situ* by vanadium-leaching regardless of used vanadium catalyst precursor.[36] This is evidenced by very similar product distributions forming by the action of very different precatalysts, as well as from indicative spectroscopic and spectrometric signatures.

In light of available data[37], the common catalyst has been suggested to be [VO(3,5-DTBC)(3,5-DTBSQ)], which is formed during catalytic turnover conditions from its catalytic resting-state $[VO(3,5\text{-DTBC})(3,5\text{-DTBSQ})]_2$, also known as Pierpont's complex.[29] The Pierpont's complex itself is derived from H_2O_2-assisted leaching of virtually any vanadium catalyst precursor, provided that 3,5-DTBC is present, in a so-called autoxidation-product-initiated reaction pathway.[36,38] However, there are also some reports of discrete oxidovanadium(V) catalysts where the supposed active catalyst,

allegedly not formed from metal leaching, has been identified using mass spectrometry.[20,23]

Herein we describe the synthesis and characterization of dioxidomolybdenum(VI) and -tungsten(VI) complexes (**1**, **2**) as well as the oxidovanadium(V) complex (**3**) and their application as bioinspired synthetic analogues to molybdenum oxotransferases and catechol oxidase. The syntheses of **1**–**3** involve complexation to a bulky Schiff base proligand *N*-(1,3-dihydroxy-2-(hydroxymethyl)propan-2-yl)-3,5-di-*tert*-butylsalicylaldimine ($H_4L^{Saltris}$) featuring several alcohol side-arms. The presence of non-coordinating hydrogen bond/donor acceptor moieties such as alcohols or amides in the outer coordination spheres of various complexes has been associated with heightened catalytic activities of the complexes in some oxidation reactions.[39,40] However, only **3** showed catechol oxidase-like activities, forming 3,5-di-*tert*-butyl-1,2-benzoquinone (3,5-DTBQ) and 4-*tert*-butyl-1,2-benzoquinone (4-TBQ), respectively. Moreover, mechanistic studies with regard to vanadium-catalyzed catechol oxidation were performed to further elaborate on the nature of the active catalyst.

Experimental

All syntheses, experiments and manipulations were run in an ambient atmosphere. $[MoO_2(acac)_2]$ (acac = acetylacetonato) and $[W(eg)_3]$ (eg = ethane-1,2-diolato = ethylene glycolato) were prepared according to known methods.[41,42] Other reagents and solvents were purchased from commercial sources and used as received. IR spectra were recorded using a Bruker VERTEX 71 FTIR spectrophotometer equipped with a RT-DLaDTGS detector. 64 scans were performed in the ATR mode for individual measurements using a Harrick VideoMVP accessory. In this setup, the sample is pressed against a diamond anvil. All data were recorded in transmittance mode with a resolution of 4 cm^{-1}. The UV-Vis measurements were performed in MeOH, MeCN and $CHCl_3$ using a Ø 1 cm quartz cuvette on an Agilent CARY60 spectrophotometer. High-resolution mass spectra were recorded on a Bruker Daltonics MicroTOF-Q II electrospray ionization time-of-flight (ESI-TOF) mass spectrometer using both negative and positive polarization as well as in MSMS mode. Full UV-Vis, NMR, IR and ESI-MS spectra are given in the supplementary material. The ^{1}H, ^{13}C, ^{19}F and ^{51}V spectra were recorded on either Bruker Avance III 600 MHz (^{1}H: 600.16 MHz, ^{13}C: 150.91 MHz) equipped with a CryoProbe Prodigy triple resonance inverse (TCI) probe or Bruker Avance 500 MHz (^{1}H: 500.08 MHz ^{13}C: 125.75 MHz, ^{19}F: 470.55 MHz, ^{51}V: 131.54 MHz) equipped with a broad-band observe probe (Bruker BBO-5 mm-Zgrad). All ^{1}H and ^{13}C NMR spectra are reported in ppm downfield relative to tetramethylsilane (TMS, δ = 0.00 ppm) and referenced to residual solvent signals $CHCl_3$-H (^{1}H: δ 7.26, ^{13}C: δ 77.16), DMSO-H6 (^{1}H: δ 2.50, ^{13}C: δ 39.52), acetone-H6 (^{1}H: δ 2.05, ^{13}C: δ 206.26, 29.84) if TMS is not present.[43] The 0 ppm fluorine and vanadium reference frequencies were calculated from the TMS ^{1}H frequency using the unified chemical shift scale by IUPAC (Ξ(^{19}F, CCl_3F) = 94.094011) and (Ξ(^{51}V, $VOCl_3$) = 26.302948), respectively.[44]

Syntheses

***N*-(1,3-dihydroxy-2-(hydroxymethyl)propan-2-yl)-3,5-di-*tert*-butylsalicylaldimine ($H_4L^{Saltris}$).** The proligand was synthesized according to a published procedure with slight modifications.[28] Detailed synthetic procedure is disclosed in the ESI. Yield: 3.08 g (91 %). ^{1}H NMR (DMSO-*d6*, 298 K, 600 MHz, TMS) δ 14.90 (1H, d, *J* = 2.2 Hz, ArO<u>H</u>,), 8.55 (1H, d, *J* = 2.2 Hz, Ar—C<u>H</u>=N—CR$_3$), 7.27 (1H, d, *J* = 2.5 Hz, Ar<u>H</u>), 7.22 (1H, d, *J* = 2.5 Hz, Ar<u>H</u>), 4.70 (3H, t, *J* = 5.4 Hz, NC—(CH$_2$O<u>H</u>)$_3$), 3.62 (6H, d, *J* = 5.4 Hz, NC—(C<u>H$_2$</u>OH)$_3$), 1.37 (9H, s, *t*-Bu), 1.27 (9H, s, *t*-Bu). ^{13}C NMR (DMSO-*d6*, 298 K, 600 MHz, TMS) δ 165.37, 160.21, 138.12, 136.18, 126.57, 125.98, 117.49, 66.80, 61.41, 34.55, 33.78, 31.32, 29.29. IR/cm^{-1} ATR mode: ν 3500–3000vb (ROH, ArOH, R(CH$_2$OH)$_3$), 2958–2868s (C–H, *t*-Bu), 1620s (RCH=N), 1593–1361m (arom. C=C), 1252m (C—O, ArOH), 1049vs, 1038vs (C—O, R(CH$_2$OH)$_3$), 882m, 644s.

[$MoO_2(H_2L^{Saltris})$], 1. 337 mg (1.0 mmol) $H_4L^{Saltris}$ and 326 mg (1.0 mmol) [$MoO_2(acac)_2$] were dissolved in 15 mL MeOH in a 50 mL Erlenmeyer flask equipped with a magnetic stir-bar. The clear yellow reaction mixture was stirred at RT for 72 hours, after which it was transferred to a –25 °C freezer. In a week, single crystals suitable for XRD had formed and were subsequently isolated by Büchner filtration, washed with small amounts of ice-cold MeOH, and air-dried to afford the analytically pure target complex. Yield: 340 mg (73 %). ^{1}H NMR (DMSO-*d6*, 298 K, 600 MHz, TMS) δ 8.49 (1H, s, Ar—C<u>H</u>=N—CR$_3$), 7.47 (1H, d, *J* = 2.5 Hz, Ar<u>H</u>), 7.44 (1H, d, *J* = 2.5 Hz, Ar<u>H</u>), 4.95 (2H, t, *J* = 5.5 Hz, NRC—(CH$_2$O<u>H</u>)$_2$), 4.43 (2H, s, NR$_2$C—(C<u>H$_2$</u>O$^-$)), 3.73 (2H, dd, *J1* = 11.3 Hz, *J2* = 5.5 Hz, NRC—(C<u>H$_2$</u>OH)$_2$), 3.63 (2H, dd, *J1* = 11.3 Hz, *J2* = 5.5 Hz, NRC—(C<u>H$_2$</u>OH)$_2$), 1.37 (9H, s, *t*-Bu), 1.29 (9H, s, *t*-Bu). ^{13}C NMR (DMSO-*d6*, 298 K, 600 MHz, TMS) δ 164.72, 156.92, 140.49, 137.92, 129.20, 128.55, 120.60, 76.65, 73.69, 61.28, 48.61, 34.89, 33.97, 31.27, 29.62. IR/cm^{-1} ATR mode: ν 3500–3000vb (ROH, R(CH$_2$OH)$_2$), 2956–2866s (C–H, *t*-Bu), 1620s (RCH=N), 1562–1361m (arom. C=C), 1038vs (C—O, R(CH$_2$OH)$_3$), 1253m (C—O, ArOH), 1045s (C—O, R(CH$_2$OH)$_2$ and R(CH$_2$O$^-$)), 916vs ν_s(MoO_2)[45–48] 880vs ν_{as}(MoO_2)[45–48], 761m, 558s ν(Mo—N)[49]. UV-Vis (MeCN; λ_{max}/ nm (ε/ M^{-1} cm^{-1}) 355 (3180). ESI-HRMS$^+$ [M+Na]$^+$ calculated m/z = 488.0945, found m/z = 488.0900. ESI-HRMS$^-$ [M–H]$^-$ calculated m/z = 464.0980, found m/z = 464.1056.

1 could be also synthesized using equimolar amounts of $H_4L^{Saltris}$ and $Na_2MoO_4 \cdot 2\ H_2O$. However, excess glacial acetic acid was required, as well as overnight refluxing. Yield using this methodology was also slightly reduced (277 mg, 60 %).

[$WO_2(H_2L^{Saltris})$], 2. 337 mg (1.0 mmol) $H_4L^{Saltris}$ and 330 mg (1.0 mmol) $Na_2WO_4 \cdot 2\ H_2O$ were dissolved in 15 mL MeOH in a 100 mL Erlenmeyer flask equipped with a magnetic stir-bar. The solution was treated with 1 mL glacial acetic acid, heated to boil in an oil-bath for two hours, then left to stir for 72 hours at RT. The pale reaction mixture was concentrated to *ca.* half of the original volume, filtered and transferred to +5 °C refrigerator. Upon *ca.* two weeks of storage, pale yellow microcrystals suitable for single crystal XRD had deposited. They were subsequently isolated by Büchner filtration, washed with small amounts of ice-cold MeOH and air-dried to afford the analytically pure

target compound. Yield: 258 mg (47 %). ^{1}H NMR (DMSO-*d6*, 298 K, 600 MHz, TMS) δ 8.46 (1H, s, Ar—C<u>H</u>=N—CR$_3$), 7.53 (1H, d, *J* = 2.4 Hz, Ar<u>H</u>), 7.47 (1H, d, *J* = 2.4 Hz, Ar<u>H</u>), 4.99 (2H, t, *J* = 5.4 Hz, NRC—(CH$_2$O<u>H</u>)$_2$), 4.58 (2H, s, NR$_2$C—(C<u>H$_2$</u>O$^-$)), 3.72 (2H, dd, *J1* = 11.1 Hz, *J2* = 3.4 Hz, NRC—(C<u>H$_2$</u>OH)$_2$), 3.63 (2H, dd, *J1* = 11.1 Hz, *J2* = 3.4 Hz, NRC—(C<u>H$_2$</u>OH)$_2$), 1.38 (9H, s, *t*-Bu), 1.30 (9H, s, *t*-Bu). ^{13}C NMR (DMSO-*d6*, 298 K, 600 MHz, TMS) δ 165.51, 155.81, 141.03, 138.36, 129.37, 129.06, 121.22, 76.76, 73.72, 61.17, 48.61, 34.85, 33.97, 31.26, 29.60. IR/cm^{-1} ATR mode: ν 3500–3000vb (ROH, R(CH$_2$OH)$_2$), 2958–2850s (C–H, *t*-Bu), 1621s (RCH=N), 1566–1362m (arom. C=C), 1300m (C—O, ArOH), 1048vs (C—O, R(CH$_2$OH)$_2$ and R(CH$_2$O$^-$)), 893vs $\nu_s(WO_2)$[45–48] 860vs $\nu_{as}(WO_2)$[45–48], 764m, 561s ν(W—N)[49]. UV-Vis (MeOH; λ_{max}/ nm (ε/ M^{-1} cm^{-1}) 365 (2440). ESI-HRMS$^+$ [M+Na]$^+$ calculated m/z = 574.1399, found m/z = 574.1435. ESI-HRMS$^-$ [M–H]$^-$ calculated m/z = 550.1424, found m/z = 550.2204.

2 could be also synthesized using equimolar amounts of H$_4$L^{Saltris} and [W(eg)$_3$]. The isolated yield of a 1 mmol scale synthesis was very low, only 40 mg (9 %).

[VO(HL^{Saltris})]$_2$, 3. 337 mg (1.0 mmol) H$_4$L^{Saltris} and 265 mg (1.0 mmol) [VO(acac)$_2$] were dissolved in 15 mL MeOH in a 100 mL Erlenmeyer flask equipped with a magnetic stir-bar. Upon *ca.* 15 minutes of stirring at RT, an umber-colored solid precipitated out of solution. The solid was collected by Büchner filtration, washed with *ca.* 30 mL RT MeOH, and air-dried to afford the target compound in a pure non-crystalline form. Umber-colored single crystals suitable for x-ray diffraction were obtained from hot acetonitrile solution upon slow cooling. Yield: 357 mg (89 %). ^{1}H NMR (acetone-*d6*, 298 K, 600 MHz, TMS) δ 9.08 (1H, s, Ar—C<u>H</u>=N—CR$_3$), 7.66 (1H, d, *J* = 2.5 Hz, Ar<u>H</u>), 7.53 (1H, d, *J* = 2.5 Hz, Ar<u>H</u>), 5.25 (1H, d, *J* = 14.3 Hz, NR$_2$C—(C<u>H$_A$</u>H$_B$O$^-$)$_A$), 5.13 (2H, m, NR$_2$C—(CH$_A$<u>H$_B$</u>O$^-$)$_A$ and NR$_2$C—(C<u>H$_A$</u>H$_B$O$^-$)$_B$), 4.70 (1H, d, *J* = 8.9 Hz, NR$_2$C—(CH$_A$<u>H$_B$</u>O$^-$)$_B$), 4.58 (1H, t, *J* = 5.4 Hz, NR$_2$C—(CH$_2$O<u>H</u>)$_C$), 4.04 (2H, dd, *J1* = 5.6 Hz, *J2* = 3.2 Hz, NR$_2$C—(C<u>H$_2$</u>OH)$_C$), 1.51 (9H, s, *t*-Bu), 1.35 (9H, s, *t*-Bu). ^{13}C NMR (acetone-*d6*, 298 K, 600 MHz, TMS) δ 165.46, 160.98, 141.26, 137.84, 131.29, 129.74, 121.38, 85.88, 81.87, 79.65, 64.51, 35.99, 34.84, 31.70, 30.45. ^{51}V NMR (acetone-*d6*, 298 K, 600 MHz, VOCl$_3$) δ –562. IR/cm^{-1} ATR mode: ν 3571w (ROH), 2954–2864s (C–H, *t*-Bu), 1623s (RCH=N), 1556–1360m (arom. C=C), 1303m (C—O, ArOH), 1075s, 1030s (C—O, R(CH$_2$OH)$_2$ and R(CH$_2$O$^-$)), 893vs ν(V=O)[19,22,50]. 853m, 764m, 552s. UV-Vis (MeCN; λ_{max}/ nm (ε/ M^{-1} cm^{-1}) 520 (550). ESI-HRMS$^+$ [M+Na]$^+$ calculated m/z = 825.2718, found m/z = 825.2599. ESI-HRMS$^-$ [M + Cl]$^-$ calculated m/z = 837.2508, found m/z = 837.2273.

3 could be also synthesized using equimolar amounts of H$_4$L^{Saltris} and VOSO$_4$ · 5 H$_2$O, with two equivalents of Et$_3$N added as a base. Similarly to the synthesis involving [VO(acac)$_2$], an umber solid was quickly precipitated out of solution, however, with a slightly lowered yield; a 1.0 mmol scale synthesis yielded 277 mg of the target compound, corresponding to a yield of 69 %.

X-ray crystallography

Single crystal X-ray data were collected using Rigaku Oxford diffraction SuperNova diffractometer equipped with micro-focus single-source (Mo-Kα radiation, λ = 0.71073 Å) and Eos detector. Data collection and processing were done using CrysAlis^{Pro}[51] software. Crystal structures were solved and refined within Olex^2[52] GUI using SHELXS[52] and SHELXL[53] programs, respectively. Atoms heavier than H were located from the difference density map and refined anisotropically. All C—H atoms were calculated to their ideal positions and refined using a riding model with the isotropic displacement parameters fixed to values corresponding to 1.2–1.5 times the U_{aniso} of the respective host atom. O—H hydrogen atoms that participate in hydrogen bond interactions were located from the difference density map and refined isotropically without restrictions in displacement parameters. The single crystal X-ray data for **1**–**3** are given in ESI table S1. Crystallographic data for the compounds reported in this paper were deposited with the Cambridge Crystallographic Data Centre, CCDC, 12 Union Road, Cambridge CB21EZ, UK. These data can be obtained free of charge on quoting the depository number CCDC 1959437–1959439 (E-Mail: deposit@ccdc.cam.ac.uk, http://www.ccdc.cam.ac.uk). The powder x-ray diffraction measurements were performed using a Huber G670 detector (Cu-Kα radiation, λ = 1.5406 Å). For each individual measurement, the exposure time was set to 30 min and with a total of 10 scans.

Cyclic voltammetry

The cyclic voltammetry electrochemical measurements of **1**–**3** (c = 1 × 10^{-3} M) were performed using a standard three-electrode setup using an Autolab PGSTAT101 potentiostat. The CVs were recorded at RT using Ø 1 mm platinum and glassy carbon (GC) working electrodes. Before use both working electrodes were polished using 6, 3, 1 and 0.25 µm diamond paste, and rinsed with quartz distilled water and technical ethanol. The quasi-reference electrode was an Ag/AgCl wire, and it was calibrated against the ferrocene redox-couple (Fc/Fc^+) ($E_{1/2}(Fc/Fc^+)$ = 0.55 V).[54] A coiled platinum wire was employed as the counter electrode. Measurements were performed using 50, 100 and 200 mV s^{-1} scanning rates in dry electrochemical grade acetonitrile with 0.1 M tetrabutyl-ammonium tetrafluoroborate ($TBABF_4$) as the supporting electrolyte. Prior to every measurement, the sample solutions were bubbled with dry N_2 for 10 minutes. The electrochemical window was –2.5 – 2.5 V for GC working electrode, and –0.8 – 2.3 V for Pt electrode, respectively.

Oxygen atom transfer reactions

All complexes were preliminarily assessed in the formal oxygen atom transfer (OAT) reactions of tris(4-fluorophenyl)phosphine ($P(p\text{-}C_6H_4F)_3$) to the corresponding tris(4-fluorophenyl)phosphine oxide ($P(p\text{-}C_6H_4F)_3O$).[55] In the OAT experiments, 500 µL of 5 × 10^{-3} M $P(p\text{-}C_6H_4F)_3$ in DMSO-H6 solution and 500 µL of 5 × 10^{-4} M **1**–**3** in DMSO-H6 solution were combined in an screw-capped scintillation vial and maintained for 24 hours at 60 °C in a thermal oven. Additionally, a control reaction involving 1000 µL 5 × 10^{-3} M

P(p-$C_6H_4F)_3$ in DMSO-H6 solution was also run. In all cases, the conversion was assessed by ^{19}F NMR and after the 24-hour period. All measurements were run in duplicate and the results obtained are given as the average of the two reactions.

Oxidation of 4-TBC and 3,5-DTBC

The oxidations of 4-TBC and 3,5-DTBC to 4-TBQ and 3,5-DTBQ were monitored by *in-situ* UV-Vis spectroscopy on an Agilent Cary 60 UV-Vis spectrophotometer and a ∅ 1.00 cm quartz cuvette. All measurements were run in duplicate and conducted at room temperature (25 °C) under ambient atmosphere. The reaction kinetics were assessed using the method of initial rates. For this, a 1.00×10^{-5} M solution of precatalyst **3** was prepared in $CHCl_3$. The substrate concentration was varied 1000, 2000, 3000, 4000, 6000, 8000 and 10000-fold relative to the catalyst to evaluate the substrate dependence of the reactions for 4-TBC. In the case of 3,5-DTBC, substrate concentration ratios of 12500, 15000 and 17500 were additionally used. The reactions were initiated directly in the quartz cuvette by combining 1.500 mL precatalyst solutions and 1.500 mL of 1.75×10^{-1} M – 1.00×10^{-2} M substrate solutions. Accordingly, final concentrations of [cat] = 5.00×10^{-6} M and [S] = 8.75×10^{-2} M – 5.00×10^{-3} M, respectively, were obtained during catalysis. The progress of the reaction was monitored by following the increase in the absorbance at *ca.* 388 nm due to 4-TBQ and 3,5-DTBC (ε(4-TBQ) = 1150 M^{-1} cm^{-1} and ε(3,5-DTBQ) = 2200 M^{-1} cm^{-1})[56,57] for 10 minutes at every one-minute interval. Absorbance *vs.* time graphs were plotted, and initial reaction rates at every concentration were determined directly utilizing the on-board Cary WinUV Kinetics software. Finally, the initial reaction rates and the substrate concentrations were fitted, using Origin 2015 software, to the Michaelis–Menten equation (1) using non-linear regression analysis, in order to obtain the maximum reaction rate V_{max}, Michaelis constant K_M ([S] at ½V_{max}) and turnover frequency k_{cat} values. The turnover frequency was calculated using the formula (2), where [E_T] is the catalyst concentration.

$$v = \frac{V_{\max} \times [\mathrm{S}]}{K_{\mathrm{M}} + [S]} \qquad (1)$$

$$k_{\mathrm{cat}} = \frac{V_{\max}}{[E_T]} \qquad (2)$$

Iodometric assay

Hydrogen peroxide was determined from the catechol oxidation reaction mixture based on I_3^-, which has a characteristic UV-Vis absorbance at *ca.* 353 nm in water. A 100 mL Erlenmeyer flask was charged with *ca.* 1 g 4-*tert*-butylcatechol and dissolved in 30 mL $CHCl_3$. 1 mol-%, or *ca.* 48 mg **3** was added to the reaction mixture, which was subsequently stirred for several days at RT. Afterwards, the reaction mixture was extracted with 25 mL distilled water. The aqueous phase was adjusted to a pH ~ 2 with dilute aqueous H_2SO_4, and a portion of it was treated with *ca.* 0.32 M KI (aq) solution and was allowed to react overnight. I_3^- was observed by UV-Vis spectroscopy at *ca.* 353 nm, whereas no such signal was observed for the bare KI solution, which was allowed to react

with atmospheric oxygen overnight. Additionally, to further confirm the presence of hydrogen peroxide, a portion of the KI solution was treated with excess amounts of 30 % aqueous H_2O_2, and the formation of a 353 nm band was again observed (ESI Figure S57)

Mechanistic catechol oxidation investigations

The UV-Vis spectroscopic investigations were performed in 1 cm quartz cuvettes by combining 1.500 mL 0.100 M 4-TBC chloroform solution containing 0.010 M BHT, DMSO or H_2O_2, and 1.500 mL chloroform solutions consisting of 1×10^{-4} M **3**. For H_2O_2 tests, 0.020 and 0.030 M solutions were additionally used. For control reactions, 0.100 M 4-TBC reacts with 0.030 M H_2O_2 in the absence of **3** (control 1), and 0.100 M 4-TBC reacts with 1×10^{-4} M **3** in the absence of H_2O_2 (control 2). The initial reaction rates were determined using the on-board Cary WinUV Kinetics software as described above. All measurements were repeated once, and the results given in figure 7 represent average values obtained from the two measurements.

For ^{51}V NMR and ESI-HRMS studies, 6 mg of **3** was suspended in 650 µL $CDCl_3$ and treated with 100 equivalents of 3,5-DTBC (166 mg) or 4-TBC (124 mg) to reflect the stoichiometry of the kinetic catechol oxidation experiments. Prior to measurements the solutions were filtered through a small cotton plug to remove any undissolved solids. ^{51}V NMR measurements were performed immediately after filtration. The same $CDCl_3$ solutions were diluted in MS grade acetonitrile, and subsequently analyzed by ESI-HRMS immediately after the ^{51}V NMR measurements.

To determine the product distribution in the oxidation of 3,5-DTBC, 500 mg of 3,5-DTBC and 18 mg of **3** (1 mol-%) were allowed to react in 30 mL boiling chloroform under ambient atmosphere overnight for *ca.* 16 hours in a 50 mL round-bottomed flask equipped with a magnetic stir-bar and a reflux condenser. Afterwards, the reaction mixture was analyzed by TLC on silica plates with technical DCM. Three components with Rf-values *ca.* 0.85, 0.58 and 0.33 were detected. The compounds were isolated by column chromatography on silica gel (technical DCM), and identified with ^{1}H, ^{13}C NMR and positive mode ESI-HRMS according to published data (ESI).[35]

Results and discussion

Syntheses and characterization of complexes

The ligand precursor $H_4L^{Saltris}$ was synthesized according to a slightly modified procedure.[28] We were also interested in the corresponding $H_5L^{Saltris}$ amine analogue, but our attempts to obtain it through reductive amination from $H_4L^{Saltris}$ proved unsuccessful. However, Mannich reaction did provide the target compound, although unselectively, and with trace yields only. Accordingly, complexations were not tested with $H_5L^{Saltris}$. The Mannich reaction including the product distribution is presented the electronic supplementary information (Scheme S1). The spectral data of all products are also listed in the ESI.

$H_4L^{Saltris}$ reacts with equimolar amounts of molybdenum precursors $[MoO_2(acac)_2]$ or $Na_2MoO_4 \cdot 2\ H_2O$ in methanol to afford *cis*-$[MoO_2(H_2L^{Saltris})]$ (**1**) as a yellow crystalline solid, whereas the use of $[MoO_2(acac)_2]$ provides slightly better yields. Likewise, the tungsten precursor $[W(eg)_3]$[42] gave *cis*-$[WO_2(H_2L^{Saltris})]$ (**2**) in methanol as pale crystals, although the (isolated) yield was very low. However, $Na_2WO_4 \cdot 2\ H_2O$ can be used to obtain **2** in a moderate yield. Vanadium precursor $[VO(acac)_2]$ rapidly reacts with $H_4L^{Saltris}$ in methanol at RT to form an umber-colored precipitate in a high yield. The solid can be crystallized from hot acetonitrile to yield analytically pure **3** with a formula $[VO(HL^{Saltris})]_2$. The schematic representation of the complex syntheses is given in scheme 1.

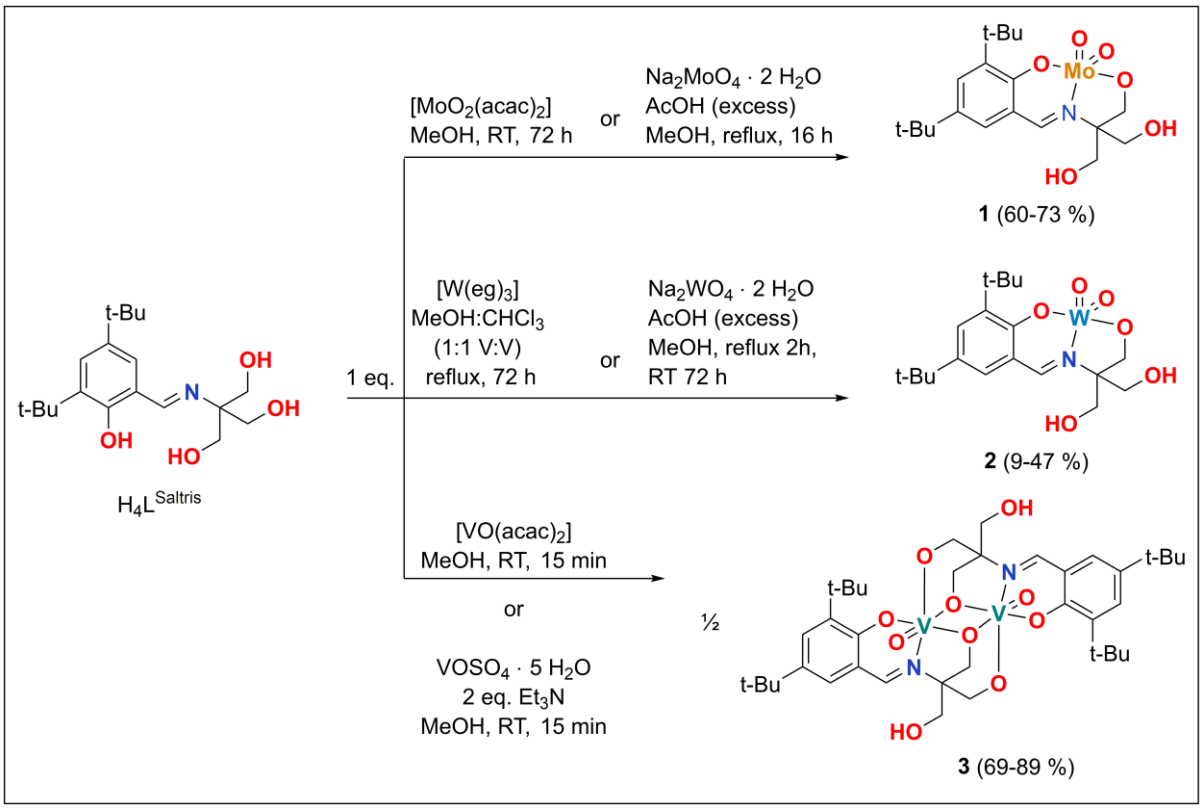

Scheme 1. Detailed description of the syntheses of **1**–**3**.

All complexes were fully characterized by means of high-resolution electrospray ionization time-of-flight mass spectrometry in positive and negative ionization modes, also utilizing MSMS. Characteristic to all complexes in the positive ionization mode is the presence of multiple singly charged sodium adducts of the type $[M - nH + (n+1)Na]^+$, where n = 1, 2, 3. In these species the protons in the trisbase alcohol arms of the complexes are sequentially substituted by sodium ions. However, singly protonated adducts of the type $[M + H]^+$ are generally not observed. Other common adducts in the positive ionization are singly charged oligomerized adducts of general type $[nM+Na]^+$, where n = 1, 2, 3. These are most likely formed by electrostatic interactions, and not representative of genuine species observable outside ionizing conditions. In the negative ionization mode, the most characteristic ionization adduct is the $[M–H]^-$ from the loss of a proton. Other common adducts are chlorido adducts of the type $[M+Cl]^-$, and dealkylation adducts $[M–R]^-$, where R represent a generic alkyl or alcohol group.

Similarly to what is observed in the positive ionization mode, electrostatic oligomerization is evident in the negative mode also.

The UV-Vis spectra of $H_4L^{Saltris}$, **1**, **2** and to a certain extent **3**, are rather similar, and contain three clear electronic absorptions. All UV-Vis spectra are presented in ESI figure 14, and the spectral data has been tabulated in Table 1. By comparing the UV-Vis spectrum of $H_4L^{Saltris}$ to those of **1**–**3** it may be concluded that all signals below *ca.* 400 nm in the case of **1** and **2**, or below *ca.* 460 nm in the case of **3** are primarily of intraligand origin. While all electronic absorptions in the proligand are visible in the UV-Vis spectra of the complexes, a noticeable redshift is observed in all signals, consistent with coordination. All high-intensity ($\varepsilon \gtrsim 2000–20000\ M^{-1}\ cm^{-1}$) electronic absorptions below *ca.* 240 nm, and the second, lower energy ($\varepsilon \sim 1150–17700\ M^{-1}\ cm^{-1}$) absorptions at *ca.* 260–287 nm in all compounds are attributed to $\pi \rightarrow \pi^*$ transitions in the aromatic ring and due to extended conjugation in the salicylaldimine chromophore. The third band at *ca.* 328–363 for $H_4L^{Saltris}$, **1** and **2** is assigned to the $n \rightarrow \pi^*$ transitions ($\varepsilon \sim 40–\ 3200\ M^{-1}\ cm^{-1}$) in the aldimine functionality.[58] **3** also contains this transition, however, it is eclipsed by what are clearly multiple overlapping absorptions in the general area between *ca.* 320–460 nm. These multiple signals have been assigned as LMCT transitions, most likely attributable to alkoxido to vanadium(V) transitions.[59] A very low-intensity LMCT at *ca.* 520 nm is assigned to phenolato → V(V) ($p_\pi \rightarrow d$), with an $\varepsilon \sim 550\ M^{-1}\ cm^{-1}$.[59] The $p_\pi \rightarrow d$ transitions in **1** and **2**, although they must exist**,** are too weak to be appropriately assigned. Likewise, the alkoxido to metal LMCT bands are much weaker in **1** and **2** compared to **3**.

In the IR spectra of all compounds, a broad signal at 3100–3500 corresponds to the phenolic and/or alcoholic OH groups while a strong stretching vibration of the imine group occurs at around 1622 cm^{-1}. The complexation of Mo, W and V to $H_4L^{Saltris}$ can be substantiated from corresponding metal oxido stretching vibrations.[29] Specifically, the characteristic symmetric and asymmetric $\nu(MO_2)$ (M = Mo, W) stretches are found at 930 and 889 cm^{-1} for **1**, and at 946 and 893 cm^{-1} for **2**, respectively.[47] These are in line with what has been reported for similar dioxidomolybdenum complexes.[60] For **3**, featuring only a single oxido ligand, a characteristic ν(V=O) stretching vibration is found at 952 cm^{-1}, which is consistent with experimental values obtained for other oxidovanadium(V) complexes bearing similar ligands.[49,59] Furthermore, a low energy signal at 553 cm^{-1} can be seen, which is assigned as ν(V—N) stretch.[61] This signal is also found in **1** at 557 cm^{-1} and is tentatively assigned to ν(Mo—N), since similar stretching vibrations are known in dioxidomolybdenum(VI) complexes bearing variable bidentate cysteamine-type ligands.[62] The signal seen in the IR spectrum of **2** at 562 cm^{-1} is cautiously assigned to ν(W—N) stretches by virtue of similarity to **1**. It should be emphasized, that the strong signal in question is missing in the IR spectrum of the proligand. IR spectral data for the most characteristic signals in all compounds in presented in table 1.

Table 1. IR and UV-Vis data for $H_4L^{Saltris}$ and **1**–**3**. See text for further information

Compound	IR (cm^{-1})				
	ν(O—H)	ν(C=N)	ν(M=O)	$\nu_{asymm.}$(M=O)	ν(M—N)
$H_4L^{Saltris}$	3100–3500	1622	–	–	–
1	3100–3500	1620	930	889	557
2	3100–3500	1621	946	893	562
3	3570	1623	952	–	553

Compound	UV-Vis		
	λ_{max} (nm)	ε (M^{-1} cm^{-1})	transition
$H_4L^{Saltris}$	225	≳ 2000	π → π*
	262	1150	π → π*
	328	400	n → π*
1	230	≥ 20000	π → π*
	260	16700	π → π*
	355	3200	n → π*
2	230	≥ 20000	π → π*
	274	12500	π → π*
	363	2500	n → π*
3	240	≥ 20000	π → π*
	287	17700	π → π*
	320–460	~7600–700	n → π*
	520	550	p_π → d

For $H_4L^{Saltris}$ the reported ^{1}H NMR data[28] significantly differs from that obtained by us, possibly due to the some difficulties in the measurements in the previous report. In any case, the ^{1}H and ^{13}C NMR data obtained by us are in good agreement with the expected structure of the ligand precursor and as such, we find re-publication of good NMR data warranted. Striking features in the ^{1}H NMR spectrum of $H_4L^{Saltris}$, very useful for structure determination, are the proton signals corresponding to the phenol, aldimine carbon, and tris-alcohol sidearms. The ^{1}H NMR data for $H_4L^{Saltris}$ and **1**–**3** is given in table 2.

The signal for the phenolic proton is found at 14.90 ppm, which is significantly downfield for what would generally be expected for phenols or salicylaldehydes, at around 10 ppm or below. Schiff bases derived from salicylaldehydes are known to exist as tautomers, shifting between their enolimine (OH) and ketoenamine (NH) forms, through what is known as RAHB (resonance assisted intramolecular hydrogen bonding).[63,64] The significant downfield resonance for the phenol proton in $H_4L^{Saltris}$ can be attributed to moderate de-shielding effect caused by the intramolecular hydrogen bonding to the aldimine nitrogen (ArO—H---N=R^1R^2).[64,65] Furthermore, with similar molecules the ^{13}C chemical shift of the *ipso* carbon atom connected to phenol OH is known to be sensitive to the relative tautomeric population between OH and NH forms, with lower average values of *ca.* 155 ppm, and higher average values of *ca.* 180 ppm generally being expected for OH, and NH forms, respectively.[64,65] In $H_4L^{Saltris}$ the corresponding ^{13}C NMR signal is found at 160.21 ppm in DMSO-*d6*, indicative of tautomeric equilibrium favoring the OH

form, a feature that is also common for similar compounds.[64] A small J-coupling (2.2 Hz) between the phenol-apparent and aldimine carbon proton can be seen in the ^{1}H NMR spectrum in DMSO-*d6*. In light of tautomeric equilibrium, this coupling has been shown to arise from $^{3}J_{NH,\alpha H}$ vicinal coupling between NH and CH of the ketoenamine form.[64] Small J-couplings of this type have been encountered before for similar compounds.[64] Other information, particularly useful for determining coordination mode of $H_4L^{Saltris}$ to various metals, are the proton signals of the tris-alcohol sidearms. In $H_4L^{Saltris}$ the three alcohol protons are clearly visible at δ 4.70, as a triplet, with a $^{3}J_{HH}$ = 5.4 Hz coupled to the six vicinal methylene protons, appearing as a duplet, at δ 3.62 ($^{3}J_{HH}$ = 5.4 Hz) when relatively dry DMSO-*d6* is used.

The coordination mode of $H_4L^{Saltris}$ to Mo, W and V was unequivocally determined by NMR in addition to single-crystal XRD. Quite unsurprisingly, the corresponding *cis*-dioxidomolybdenum(VI) and -tungsten(VI) complexes *cis*-[$MO_2(H_2L^{Saltris})$], where M = Mo or W, share analogous structures in DMSO solution as well. $H_4L^{Saltris}$, as a potentially pentadentate ligand, coordinates to both metal centers in tridentate, dianionic manner *via* the phenolato oxygen, aldimino nitrogen and one alcoholato sidearm.[66,67] The coordination mode is clearly evident from ^{1}H NMR in dry DMSO-*d6*. For example, the phenol proton at δ 14.90 is missing, and the aromatic protons have been shifted downfield, relative to $H_4L^{Saltris}$, for *ca.* 0.21 ppm and 0.26 ppm for **1** and **2**, respectively. Curiously, the signal corresponding to aldimine CH proton is shifted upfield very slightly (< 0.10 ppm) in both complexes relative to $H_4L^{Saltris}$. These effects might be explained by inductive effects: Upon coordination of the aldimine nitrogen, its electron density is withdrawn towards the electron-deficient Mo(VI) and W(VI) centers, manifesting as a slight shielding effect for the aldimine CH proton.

As was disclosed earlier, the three alcohol protons in $H_4L^{Saltris}$ are clearly visible as a triplet, however, in the complexes these same triplets only correspond to two protons. In **1**, the triplet corresponding to two free sidearm alcohol protons is found slightly downfield relative to $H_4L^{Saltris}$ at δ 4.95 ppm, ($^{3}J_{HH}$ =5.5 Hz), whereas in **2** it is located at δ 4.99 ppm. In both complexes, the four methylene protons corresponding to the two uncoordinated alcohol sidearms appear as duplets of duplets, at δ 3.73 and 3.64 for **1**, and δ 3.72 and 3.63 ppm for **2**, respectively. Accordingly, the methylene CH_2 for the coordinated alcoholato sidearm is found, as a singlet, at δ 4.43 for **1** and δ 3.58 for **2**.

The most distinguishable feature of the ^{13}C NMR spectra for **1** and **2** relative to that of $H_4L^{Saltris}$ are the methylene CH_2 carbons in the alcohol sidearms. In **1** and **2** these become inequivalent due to expected slightly different electronic environments and steric perturbations caused by coordination to the metals. Except for the quaternary carbon connecting to the alcoholato arms and aldimino nitrogen, which is upshifted in both complexes for *ca.* 18 ppm, the alcohol and alcoholato methylene protons have been downshifted for *ca.* 15 ppm in both **1** and **2**, consistent with coordination and changes in electronic environment.

Table 2. ^{1}H NMR spectral data of $H_4L^{Saltris}$, **1**–**3** (δ in ppm). Multiplicity: s = singlet, d = duplet, t = triplet, m = multiplet (unresolved), b = broad.

Compound	ArO<u>H</u>	C<u>H</u>=N	Arom. H	NC(CH$_2$O<u>H</u>)$_3$	NC(C<u>H$_2$</u>OH)$_3$	tBu
$H_4L^{Saltris}$	14.90 (d, 1H)	8.55 (d, 1H)	7.27, 7.22 (d, 1H)	4.70 (t, 3H)	3.61 (d, 6H)	1.37, 1.27 (s, 9H)
1	–	8.49 (s, 1H)	7.47, 7.44 (d, 1H)	4.95 (t, 2H)	3.73; 3.64 (dd, 2H); (dd, 2H)	1.37, 1.29 (s, 9H)
2	–	8.46 (s, 1H)	7.53, 7.47 (d, 1H)	4.99 (bt, 2H)	3.72; 3.64 (dd, 2H); (dd, 2H)	1.38, 1.30 (s, 9H)
3	–	9.08 (s, 1H)	7.66, 7.53 (d, 1H)	4.58 (t, 1H)	5.25 (d, 1H) 5.13 (m, 2H) 4.70 (d, 1H) 4.04 (dd, 2H)	1.51, 1.35 (s, 9H)

In the oxidovanadium(V) complex **3**, $H_4L^{Saltris}$ coordinates in a tetradentate, trianionic fashion *via* phenolato, aldimino and two alcoholato groups, in stark contrast to **1** and **2**. In principle, ^{1}H NMR spectrum of **3** agrees well with a trigonal bipyramidal coordination mode, which is common for vanadium(V) complexes. In the absence of single crystal XRD and ^{51}V NMR measurements, comparable 5-coordinate solution-state structure has also been proposed for several very similar vanadium(V) complexes.[59] However, in our case, single crystal XRD reveals that **3** is dinuclear in the solid state (see discussion below), with both vanadium centers adopting a distorted octahedral coordination mode. Furthermore, ^{51}V NMR shows only one signal, which supports the dinuclear configuration in solution state as well, since both vanadium centers are chemically equivalent. Generally speaking, 5-coordinate vanadium complexes may isomerize to 6-coordinate species *via*, for example, solvent ligand exchange, and vice versa. Furthermore, 6-coordinate vanadium complexes may have multiple isomers if a solvent molecule is coordinated. These dynamics are frequently observed as multiple signals in the ^{51}V NMR, although the choice of NMR solvent may or may not greatly influence this. The single ^{51}V NMR signal supports the notion that **3** is 6-coordinate, and is rigid *i.e.* does not contain any coordinated solvent molecules in the solution state.

In **3**, the aldimine carbon proton and aromatic protons have been moderately shifted downfield for *ca.* 0.34 and 0.27 ppm, respectively, relative to $H_4L^{Saltris}$. Similarly to **1** and **2**, where the tris-alcohol sidearms become inequivalent relative to the free ligand, in **3** these changes are much more pronounced. For example, the methylene CH_2 protons for the two alcoholato sidearms, have been shifted downfield by 0.79 – 1.35 ppm. They also appear separately as diastereotopic duplets, due to formation of rigid 5- and 6-membered ring structures, respectively. The single free alcohol sidearm, on the other hand, appears 0.59 ppm downshifted for OH, and 0.13 ppm for the CH_2 protons, respectively.

The ^{13}C NMR spectrum of **3** is very similar to those of **1** and **2**. Most striking features are the collapse of the equivalent (in $H_4L^{Saltris}$) tris-alcohol carbons to inequivalent carbons in **3**, with approx. 15 ppm shift downfield observed for the two coordinating alcoholato methylene protons. Strikingly, the ^{51}V NMR spectrum of **3** shows only one signal at *ca.* –562 ppm. The simple nature of the ^{51}V NMR spectrum points towards that **3** is present, in solution, as a one stable species, and that there is probably little if any solution dynamics

commonly encountered with vanadium compounds. The ^{51}V NMR observation is well in line with single-crystal XRD results, in that the complex unit is symmetric, and both oxidovanadium(V) centers adopt rigid six-coordinate distorted octahedral configurations, making the vanadium centers chemically equivalent. The obtained ^{51}V NMR spectrum is closely similar to those of other related oxidovanadium(V) complexes.[49] Furthermore, the ^{51}V NMR signal is present in the expected general area† attributable to oxidovanadium systems bearing redox-innocent O_4N type ligands.[33,68]

Description of crystal and molecular structures

Good quality single crystals of **1**–**3** could be grown thus enabling their structural characterization by single crystal X-ray diffraction methods. **1** and **2** crystallized directly from the reaction mixtures, *i.e.* from methanol as brightly yellow needle-like crystals (**1**) and pale yellow needle-like crystals (**2**). **3**, on the other hand, deposited from the methanol reaction mixture in a non-crystalline form. Umber-colored block-like crystals could be obtained from boiling acetonitrile upon slow cooling. All three complexes crystallize in the monoclinic crystal system and have the same space group ($P2_1/c$).

The X-ray structure of **1** (Figures 1 and 2) reveals that the reaction between molybdenum precursor and $H_4L^{Saltris}$ has involved the deprotonation of two proligand OH groups – the phenolic and one of the three alcoholic OH moieties – and coordination of the respective O atoms to the dioxidomolybdenum(VI) center. The rather distorted octahedral coordination sphere of the Mo(VI) ion is fulfilled by the aldimino N donor and one of the alcoholic OH groups of an adjacent complex unit (for selected bond parameters, see Figure 1). A CSD survey[69] of dioxidomolybdenum(VI) complexes with similar trisbase salicylaldimine-type ligands reveals that in such complexes only one of the three available alcoholic groups tends to coordinate to the central metal ion, similarly to **1**. Furthermore, the remaining sixth coordination site in the previously reported complexes is occupied by a solvent molecule (H_2O, MeOH, DMF or DMSO), which leads to discrete molecular complexes. In the crystal structure of **1**, however, the distinguishable complex units couple together via Mo—$O_{alcohol}$ bonds thus creating a polymeric 1D chain along the crystallographic *b*-axis. The polymeric system is further stabilized by intrapolymer Mo=O···H—O [*d*(O2···O6') = 2.65 Å] hydrogen bonds (HB) as well as interpolymer HBs occurring *via* Mo—OH···OHCH_2CN [*d*(O5'···O6'') = 2.63 Å] contacts. It is noteworthy that, albeit being polymeric in the solid state, **1** dissolves readily in DMSO which can be attributed to the degradation of the polymeric chains into the respective monomeric complex units (see NMR analysis above). This confirms the lability of the Mo—$O_{alcohol}$ bonds and the discrete nature of the complex upon dissolution.

† V(V) complexes bearing a redox-innocent O_5N_1 donor set generally appear between *ca.* –600 to –400 ppm according to ref. [33] and at lowest *ca.* –650 ppm according to ref. [68] (δ ppm *vs.* $VOCl_3$).

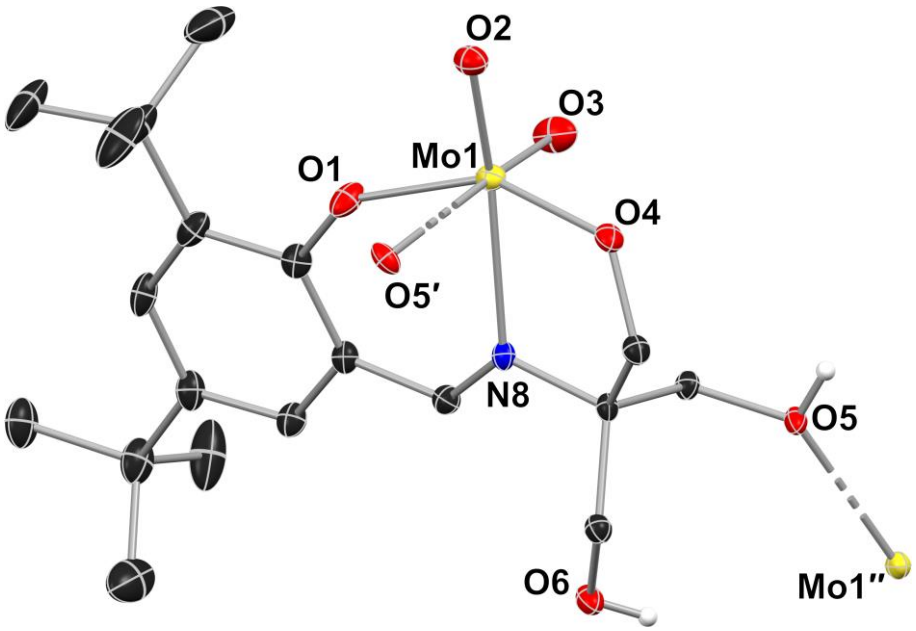

Figure 1. Presentation of the asymmetric unit of **1** with bonds to the neighboring complex units shown in dashed lines. All C—H hydrogen atoms are omitted for clarity. Principal ellipsoids are presented at the 50 % probability level. Relevant bond lengths (Å): Mo1—O1 = 1.9300(14), Mo1—O2 = 1.7237(12), Mo1—O3 = 1.6942(13), Mo1—O4 = 1.9060(13), Mo1—O5′ = 2.4123(13) and Mo1—N8 = 2.2912(14). Symmetry operations: (′) = 1-x, ½+y, ½-z; (″) = 1-x, -½+y, ½-z.

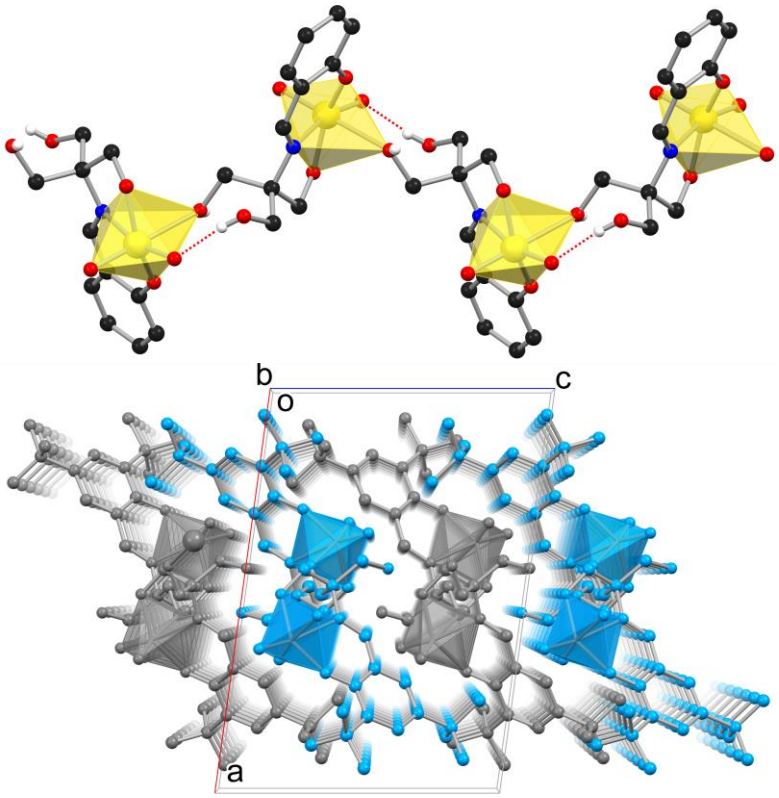

Figure 2. Partial view of the 1D polymeric structure of **1** (top) and illustration of packing of the discrete polymers (alternating blue and grey colors, below) viewed along the crystallographic *b*-axis. Top: C—H hydrogen atoms and *tert*-butyl groups omitted. Below: All hydrogen atoms omitted.

In contrast to **1**, the respective tungsten analogue **2** crystallizes as monomeric units in which the WO_2 unit is bound to a dianionic tridentate $H_2L^{Saltris}$ ligand in agreement with the NMR analyses. The remaining coordination site, which is *trans* to O3, has been taken up by a water molecule (Figure 3). Although there is one example of tungsten complex bearing a very similar ligand, the [WO_2(sapd)] (sapd = salicylidene propanediol)[70], to the best of our knowledge, **2** is the first report of a tungsten complex characterized by XRD that bears a Saltris-type Schiff base ligand. It should be noted, that the solid state structure of **2** closely resembles some known Mo-complexes‡ such bearing Saltris-like ligands.[58,71] In **2**, two of the three ligand alcoholic OH groups remain uncoordinated and are thus available for hydrogen bonding. In case of **2**, this leads to an intricate hydrogen bonding network in the crystal lattice in which the monomeric units build into 2D sheets, terminated by the aliphatic regions of the molecules (ESI, Figure S59).

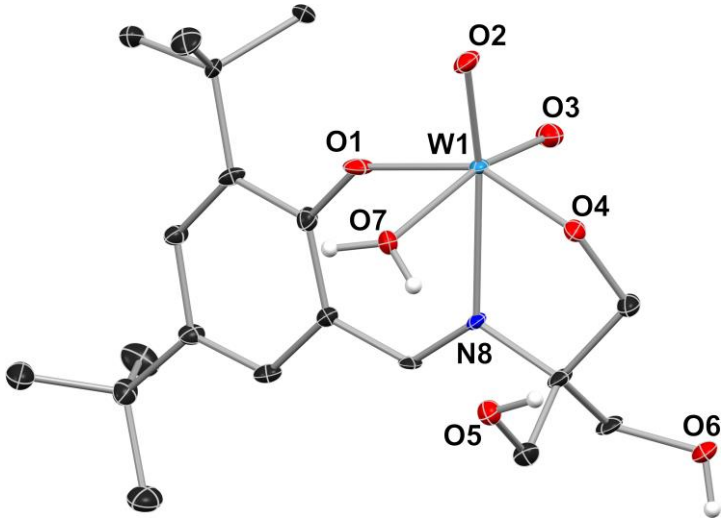

Figure 3. Illustration of the asymmetric unit of structure of **2**. All C—H hydrogen atoms are omitted for clarity. Principal ellipsoids are presented at the 50 % probability level. Relevant bond lengths (Å): W1—O1 = 1.928(4), W1—O2 = 1.764(4), W1—O3 = 1.715(4), W1—O4 = 1.902(4), W1—O7 = 2.309(4) and W1—N8 = 2.283(4).

X-ray structure of **3** shows a formation of a dinuclear vanadium complex consisting of two oxidovanadium(V) centers and two ligands wherein each ligand is coordinated in tetradentate trianionic fashion (Figure 4). The crystal structure is solved with half of the [$VO(HL^{Saltris})]_2$ dimer constituting the asymmetric unit while the complete centrosymmetric complex is generated via an inversion center between the V atoms. Also, an acetonitrile solvent molecule is located in the asymmetric unit. The crystallographically unique complex moiety comprises of oxidovanadium(V) ion chelated in ONO fashion by phenolato (O1), aldimino (N8) and alcoholato (O3) groups of $HL^{Saltris}$. The dimer is upheld by alcoholato atoms O3 and O3′, which act as bridging donors between the V(V) centers, and alcoholato atoms O5 and O5′ which coordinate to neighboring V1′ and V1, respectively. This bonding scheme yields an approximately planar (maximum deviation from planarity is ca. 17°) V_2O_6 system to which two alcoholato and two aldimino groups coordinate perpendicularly. The V—O distances in the V1—O3/O3′—

‡ Solid state structure of **2** is very similar to MoO_2 complexes **1**–**5** from ref. [58] and **1**–**3** from ref. [71].

V1′ bridges show high degree of asymmetry (ca. 0.4 Å). Structurally, **3** is very similar to some other reported dimeric vanadium complexes bearing analogous ligands.[49,66,72]

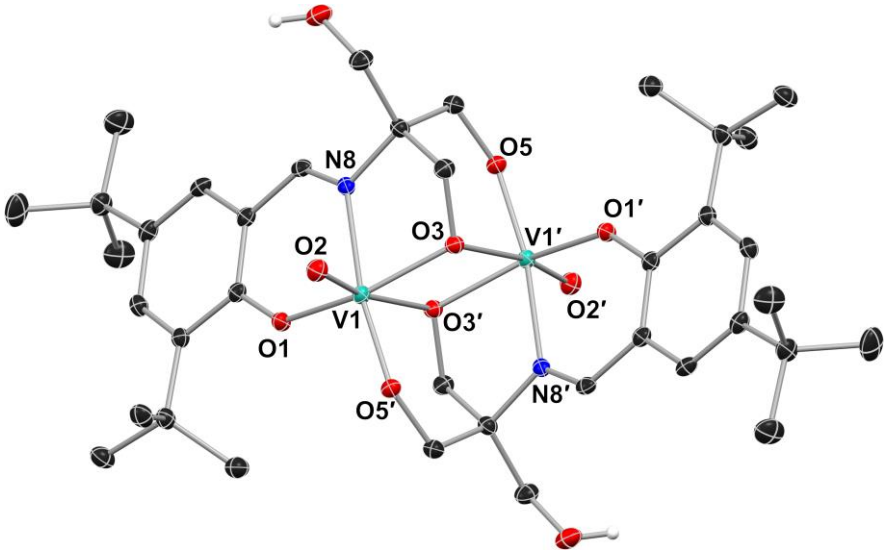

Figure 4. Presentation of the $[VO(HL^{Saltris})]_2$ complex found in the crystal structure of **3**. All C—H hydrogen atoms are omitted for clarity. Principal ellipsoids are presented at the 50 % probability level. Relevant bond lengths (Å): V1—O1 = 1.8646(12), V1—O2 = 1.6009(13), V1—O3 = 1.9028(12), V1—O3′ = 2.3066(12), V1—O5′ = 1.7981(12) and V1—N8 = 2.1323(15). Symmetry operations: (′) = -x, 1-y, 1-z.

X-ray powder diffraction analysis

Bulk samples of **1**–**3** were analyzed by powder X-ray diffraction (PXRD). The unit cell parameters of complexes **2** and **3** were determined by Pawley analysis[73] within the HighScore Plus 4.7 program using the cell parameters of corresponding single crystal structures as the starting point of the least-squares refinements. The variable parameters in the refinements were zero-offset, unit cell and peak profile parameters. The fitted diffraction graphs for **2** and **3** are found in ESI figures S61–62 whereas the refined unit cells and the resulting R-factors and goodness-of-fit values are presented in ESI table S2. For **2**, due to instrument limitations, we could not record one of the major low angle peaks which resides at ca. 4.5° according to the simulated single crystal pattern.

In case of complex **1**, the experimental PXRD pattern shows some similarities with the pattern simulated from the respective single crystal structure but it is in general distinctively different (ESI figure S60). We suspect that this may arise from a degradation of the polymeric structure of **1** while preparing the sample of PXRD analysis by grinding of the crystalline bulk material. In contrast, the unit cell parameters of bulk materials of **2** and **3**, derived from the Pawley analysis, are in good agreement with the corresponding single crystal structures and thus demonstrate their structural similarity. The refined unit cells (PXRD) show *ca.* 2 % increase in unit cell volume which is reasonable considering the thermal expansion due to the differences in data recording temperature between the single crystal and powder data (120 *vs*. 298 K)

Cyclic voltammetry

To gain insight into the reactivity of the complexes, and specifically to study the ability of **1**–**3** to undergo reversible redox-reactions relevant regarding catechol oxidation, electrochemical investigations were undertaken. The cyclic voltammograms of **1**–**3** are presented in the electronic supplementary material, while the electrochemical data has been tabulated in table 3. **3** has a reversible electrochemical response with $E_{½}$ = –415 mV with Pt working electrode, and $E_{½}$ = –422 mV using GC working electrode, respectively**.** This response has been assigned as the V(V)/V(IV) redox-couple, since it is also observed in the same potential area with some other structurally similar[§] Schiff base oxidovanadium(V) complexes.[49,59]. With higher scan rates, slight quasi-reversibility is observed, although $E_{½}$ does not change significantly. In the positive potential range three irreversible oxidation responses occur at $E_{½}$ = *ca.* +900 mV, +1.496 and +1.683 V (Pt WE), that are most likely ligand-centered, since they are also varyingly present in **1** and **2**. For example, in some unrelated complexes phenoxyl radical formation has been suggested to occur at approx. +650–750 mV.[74] Accordingly, we tentatively assign the ~ +900 mV redox-response to PhO → PhO$^{\bullet+}$, and subsequent oxidation events at higher potentials to alkoxy-centered oxidations *i.e.* RO → RO$^{\bullet+}$. The cyclic voltammograms of **1** and **2** are remarkably featureless in comparison to those of **3**. All redox-processes present in **1** and **2** are irreversible, with the one-electron reductions *e.g.* Mo(VI) → Mo(V) and W(VI) → W(V) tentatively assigned as –0.896 (Pt) and –1.296 V (GC), respectively.[66] Similar ligand-centered irreversible oxidation events are present in **1** and **2** than what is found in **3**.

Table 3. Electrochemistry data obtained for **1**–**3**.

Complex	ligand-centered *e.g.* RO → RO$^{\bullet+}$		ligand-centered *e.g.* RO → RO$^{\bullet+}$		ligand-centered *e.g.* PhO → PhO$^{\bullet+}$		metal-centered M(os)/M(os+1)	
	Pt	GC	Pt	GC	Pt	GC	Pt	GC
1	–	+2.159	+1.691	+1.717	–	+0.942	–	–0.986 irrev.
2	–	–	+1.653	+1.684	+0.934	+0.959	–	–1.296 irrev.
3	+1.683	1.682	+1.496	+1.484	+0.896	+0.917	–0.415 ps. rev.	–0.422 ps. rev.
The values are given in V *vs.* Ag/AgCl calibrated against Fc/Fc^{+} redox-couple.[54] GC and Pt represent glassy carbon and platinum working-electrodes (WE), respectively.								

Catechol oxidase mimetic activity

In various catechol oxidase studies 3,5-DTBC is the substrate of choice[19,20,28], owing to its relatively easy oxidation due to its low redox potential.[75] As such, the catechol oxidase mimetic activity of all complexes was studied in the aerial oxidation of 3,5-DTBC as well as 4-*tert*-butylcatechol (4-TBC) and pyrocatechol in chloroform, acetonitrile and

[§] Structurally related V(V) complexes such as **3** and **6**–**8** from ref [49] and **1**, **2**, **4** and **5** from ref. [59] display a V(IV)/V(V) redox couple at $E_{½}$ values –470 to –400 mV *vs.* Ag/AgCl in DMF.

methanol. 4-TBC and pyrocatechol were chosen because they are more resistant to autoxidation compared to 3,5-DTBC.

Preliminary investigations indicated that 3,5-DTBC and 4-TBC readily reacted to form the corresponding *o*-benzoquinones, namely 3,5-di-*tert*-butyl-1,2-benzoquinone (3,5-DTBQ) and 4-*tert*-butyl-1,2-benzoquinone (4-TBQ), respectively, when **3** was used as the catalyst in $CHCl_3$, MeOH and MeCN. However, **1** and **2** showed no noticeable catechol oxidase-like activity in the same time frame, although UV-Vis and ESI-HRMS measurements confirmed that the catechols coordinate to the metal centers (ESI Figures S35–S46). Furthermore, pyrocatechol was observed not to react in any solvent with any of the catalysts. With **3**, catechol coordination was also evident from the fact that all of the reaction solutions turned blue after the addition of the catechols, a characteristic color for vanadium-catecholato species[31], with also typical vanadium-catecholato LMCT bands observable in the UV-Vis spectra at *ca.* 650 and 830 nm (figure 5).[31,33,76] Furthermore, the solutions eventually turned green and finally yellow-brown due to the formation of *o*-benzoquinones. UV-Vis spectroscopic measurements confirmed the UV bands of 3,5-DTBQ and 4-TBQ, that appear at approx. 400 nm.[56,57]

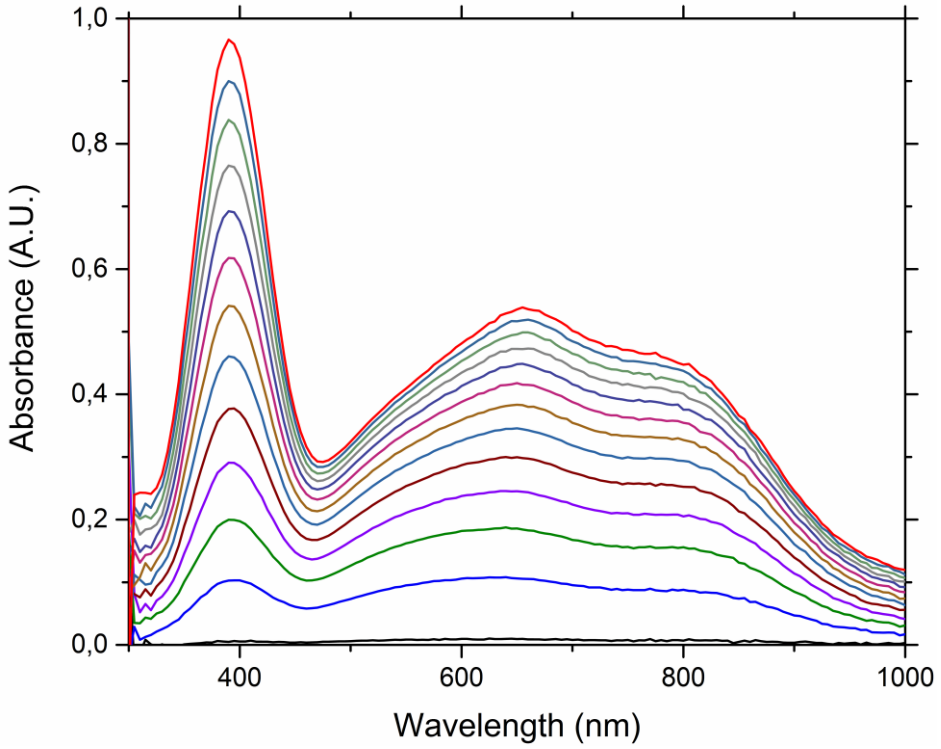

Figure 5. The formation characteristic vanadium-catecholato LMCT bands at approx. 650 and 830 nm during 3,5-DTBC oxidation by **3**. The reaction was monitored for 1 hour and spectra were recorded at every 5-minute interval.

From the kinetics data it can be concluded that the oxidation of 4-TBC and 3,5-DTBC catalyzed by **3** follows typical Michaelis–Menten like kinetics (figure 6). At low substrate concentrations, the measured absorbance increases linearly as a function of time, indicative of a first order reaction with respect to the substrate. However, upon significant excess (> 10 000-fold) of the substrate relative to catalyst the reaction rate

becomes pseudo zero-order. At this regime subsequent substrate additions will not speed up the reaction, as the catalyst becomes saturated. The kinetic parameters V_{max} (maximum reaction rate), Michaelis-constant K_M ([S] at ½V_{max}) and k_{cat} (turnover frequency) are given in table 4. From the kinetics data it can be seen that **3** compares well with other oxidovanadium systems, with its catalytic activity falling well within the range of that of others (table 4).[18–21] However, the most remarkable aspect is the fact that **3** offers a comparable catechol oxidase-like activity to the structurally very similar dicobalt complex $[Co(H_2L^{Saltris})(OAc)]_2$.[28]

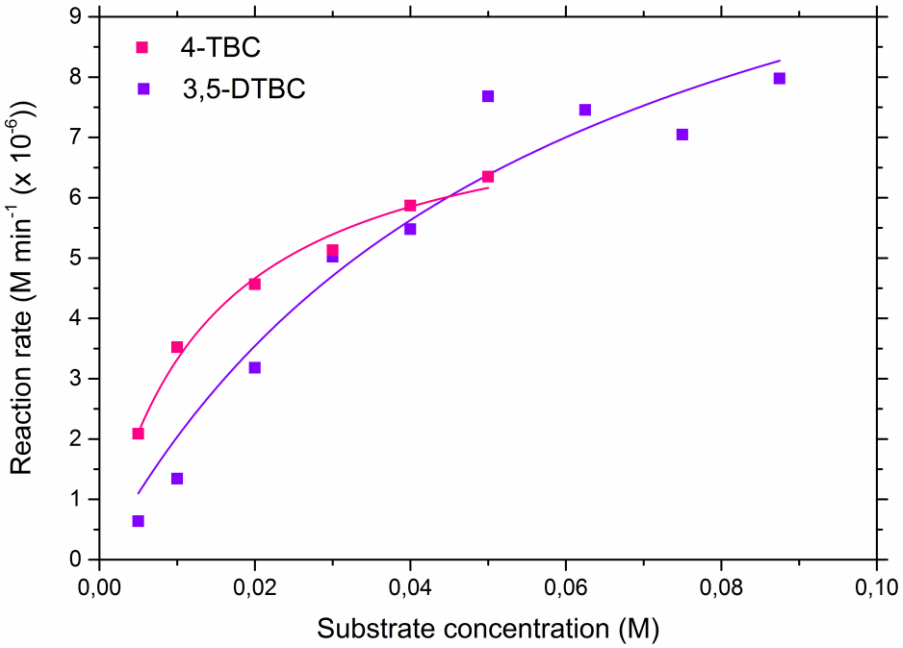

Figure 6. Michaelis–Menten plots of the oxidations of 4-TBC and 3,5-DTBC by **3** in $CHCl_3$.

While the natural catechol oxidase catalyzes the oxidation of catechols to corresponding *o*-benzoquinones, producing water[15] as the sole by-product, a number of model transition metal complexes produce hydrogen peroxide as well.[28,77–81] Recently, a dicobalt complex $[Co(H_2L^{Saltris})(OAc)]_2$ structurally strikingly similar (lacking oxido ligands) to **3** was assessed in the oxidation of 3,5-DTBC.[28] Mechanistic investigations involving MS measurements strongly hint towards a single and double 3,5-DTBSQ adducts $[(Co(III)(HL^{Saltris})Co(II)(H_2L^{Saltris})(3,5\text{-DTBSQ})]$ and $[Co(II)(H_2L^{Saltris})(3,5\text{-DTBSQ})]_2$. Some studies highlight the importance of metal–metal distance, which may give insights into the overall catalytic mechanisms of any given catechol oxidase model system.[78,79] In light of the obvious structural similarities between the dinuclear cobalt(III) complex and our dinuclear oxidovanadium(V) complex, as well as the fact that there are only a limited[20,23] mechanistic investigations on catechol oxidation involving modern oxidovanadium systems, we conducted mechanistic investigations of our own using UV-Vis, ^{51}V NMR and ESI-HRMS spectrometry. The detailed descriptions of the experiments are given in supplementary material.

Table 4. Catechol oxidation results for the present $[VO(HL^{Saltris})]_2$ as well as some other selected vanadium-based catechol oxidase mimetic systems.

Compound	k_{cat} (h^{-1})	K_M (M)	V_{max} (M min^{-1})	Ref.
3	164∓32[a]	0.05727	1.37×10^{-5}	This work
3	94∓4[b]	0.01363	7.84×10^{-6}	This work
$[VO(L^1)]_2 SO_4$	1439[bc]	–	–	[18]
$[VO(OMe)(L^2)]$	12[a]	0.00115	1.01×10^{-5}	[21]
$[VO(OMe)(L^3)]$	13[a]	0.00107	1.04×10^{-5}	[21]
$[VO(OMe)(MeOH)(L^4)]$	3[a]	0.00557	7.66×10^{-6}	[19]
$[Co(H_2L^{Saltris})(OAc)]_2$	80[a]	0.0087	1.33×10^{-5}	[28]
$[VO_2(L^5)]$	2063[a]	0.00079	5.73×10^{-5}	[20]
$[VO(L^6)]$	395[a]	0.00103	6.58×10^{-3}	[23]

[a] = For oxidation of 3,5-DTBC. [b] = For oxidation of 4-TBC. [c] = In the presence of stoichiometric amounts of base (Et_3N).

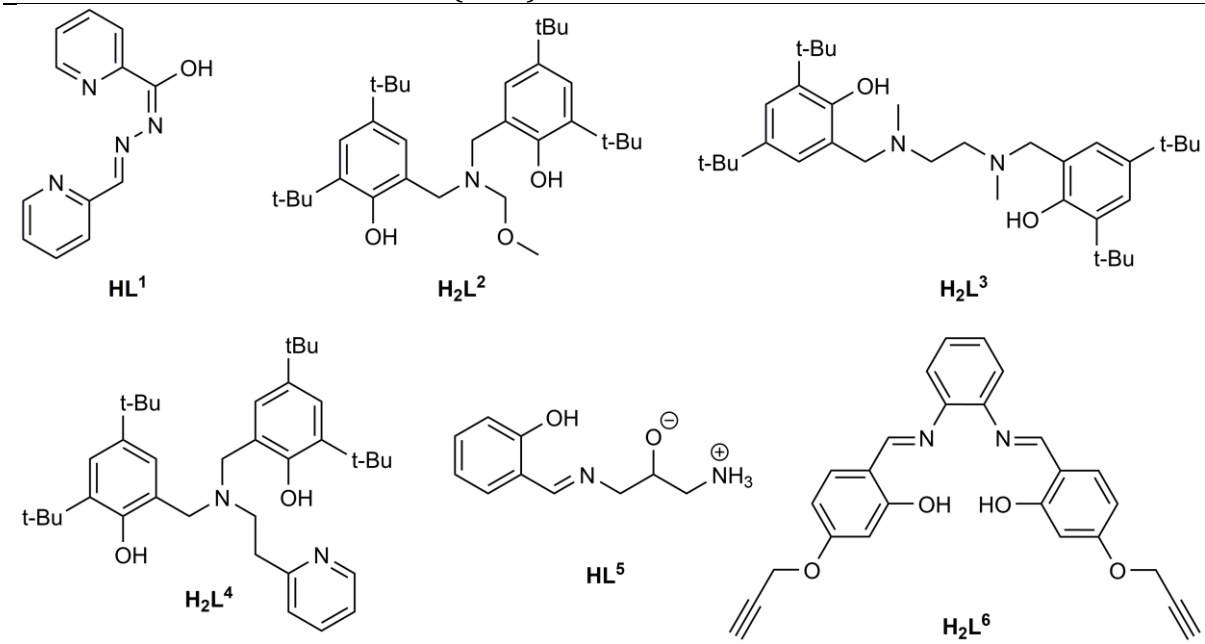

The initial reaction rate of the oxidation of 4-TBC by 0.1 mol-% of **3** was measured by UV-Vis spectroscopy in the presence of DMSO (hydroxyl radical quencher), BHT (butyrated hydroxytoluene, radical inhibitor), and varying concentrations of H_2O_2 in chloroform (figure 7). The addition of DMSO or BHT (entries 3 and 4) have little effect on the initial reaction rate when compared to the effects of **3** alone (entry 2), so it may be concluded that hydroxyl radicals or any other radicals most likely do not significantly contribute to the overall oxidation mechanism. However, hydrogen peroxide seems to accelerate the oxidation to some extent in the presence of **3**, with reaction rate increasing approx. linearly with increasing H_2O_2 concentration (entries 5–7). However, and importantly, even in relatively high concentrations H_2O_2 does not significantly oxidize 4-TBC in the absence of **3** (entry 1), so the reaction rate enhancement most probably does not come from the direct substrate oxidation by H_2O_2. Indeed, it has been previously shown that

H_2O_2 may assist the dissociation, or leaching, of vanadium from vanadium-containing species, which then rapidly convert to catalytically active catecholato-bearing vanadium species *e.g.* [VO(3,5-DTBC)(3,5-DTBSQ)] and [V(3,5-DTBC)$_3$] in the presence of very large excess of catechol, 3,5-DTBQ and H_2O_2 relative to vanadium.[36,38] In a separate experiment, an iodometric assay was done to confirm the formation of hydrogen peroxide in our system.

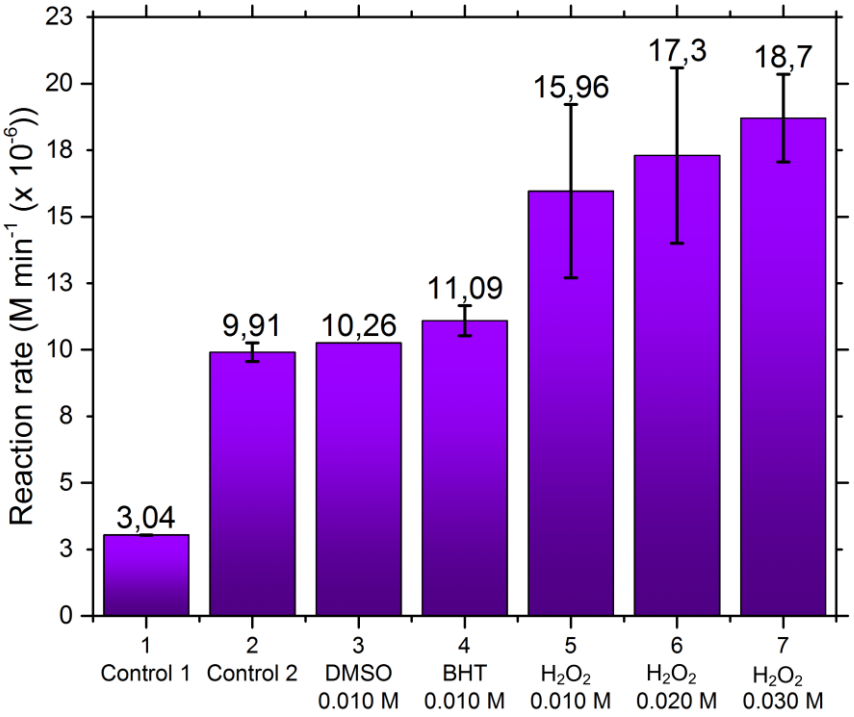

Figure 7. Initial reaction rate of 4-TBC (0.1 M) oxidation over the period of 20 minutes in the presence of **3** (1×10^{-4} M) and/or several additives. See text for further information. Control 1: 0.1 M 4-TBC + 0.030 M H_2O_2 in the absence of **3**. Control 2: 0.1 M 4-TBC + **3** in the absence of H_2O_2. All measurements run in duplicate.

^{51}V NMR experiments were undertaken to determine qualitatively the nature of vanadium-containing species formed during catechol oxidation, and to gain some insight into the catalytically active vanadium species. In the experiments, 100 equivalents of 3,5-DTBC and 4-TBC were reacted with **3** in $CDCl_3$ at RT, and the ^{51}V NMR spectra were recorded immediately. The ^{51}V NMR spectra obtained from these experiments drastically differed from the original ^{51}V NMR spectra of **3** (figure 8). In both cases, the original signal corresponding to **3** at *ca.* –562 ppm vanished completely, which is a clear indication of dynamic and very rapid changes to the first coordination sphere of **3**. New, very broad signals were observed at *ca.* +1221 and +1185 with 4-TBC and at *ca.* +1391 with 3,5-DTBC *viz.* significantly downfield relative to $VOCl_3$.

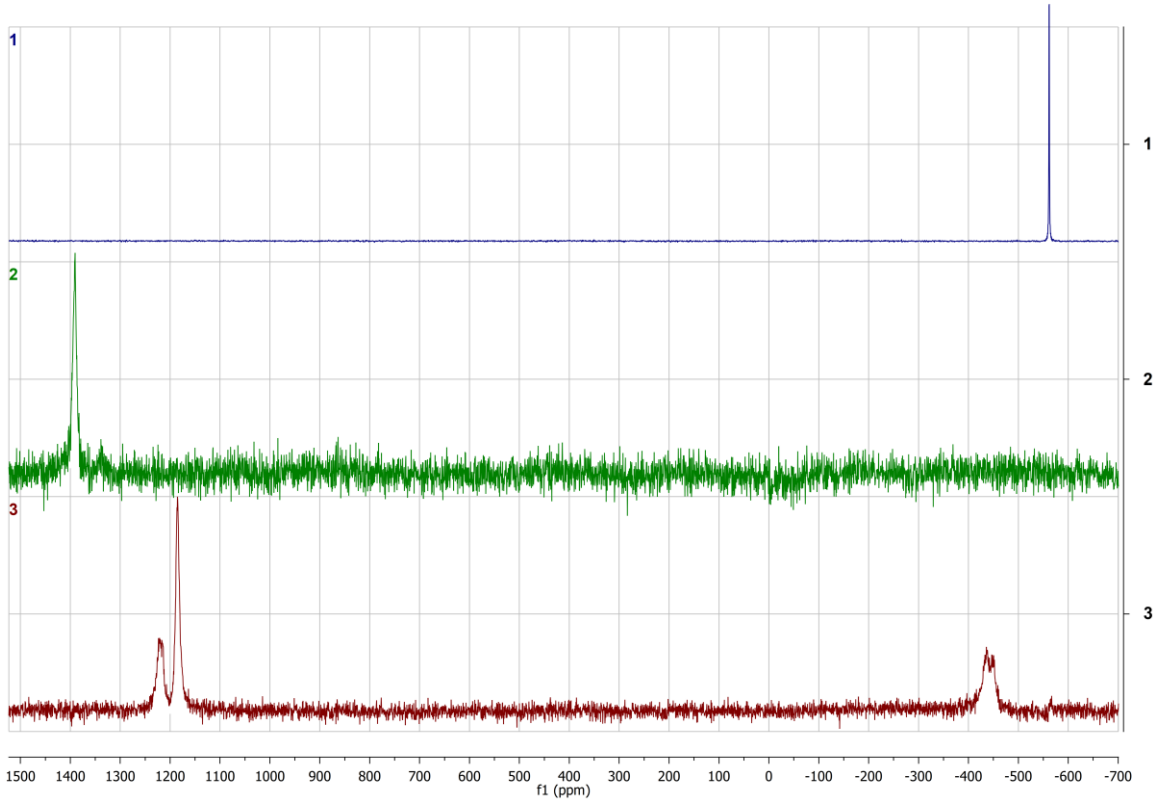

Figure 8. ^{51}V NMR spectra of 1) **3** in acetone-*d6*., 2) **3** + 100 eq. 3,5-DTBC in $CDCl_3$. and 3) **3** + 100 eq. 4-TBC in $CDCl_3$.

These prominent changes, and the absence of ^{51}V NMR signals at approx. –400 – (–600) ppm, the expected region for oxidovanadium(V) complexes bearing a redox-innocent NO_5 donor set, indicate that there are most likely no vanadium species bearing $HL^{Saltris}$ left.[33,68] In fact, the significantly downfield signals are almost certainly related to diamagnetic catecholato-bearing vanadium species with at least two or even three catechol ligands, since many reported non-innocent monocatecholato oxidovanadium(V) systems with mixed ON donors appear upfield, and at best only slightly downfield of $VOCl_3$.[33] It should be noted, that the ^{51}V NMR spectra did not drastically change over a period of two days. Furthermore, when 4-TBC was used a signal was observed at –438 ppm, only slightly downfield of **3**. This species has been tentatively assigned to [(VO($HL^{Saltris}$)(*O*-4-TBC)], where 4-TBC coordinates in a singly anionic monodentate fashion. These assignments are in line with observations from ESI-MS studies (see below), where bis- and tris(catecholato) oxidovanadium and non-oxidovanadium species are detected.

To supplement the rather cautious assignments done in the ^{51}V NMR section above, the same NMR samples were analyzed by ESI-HRMS in acetonitrile. Some reported mechanistic studies investigating catechol oxidation by oxidovanadium complexes frequently involve ESI-MS only in the positive mode.[20,23] However, as per the findings by Finke and co-workers related to the nature of the true active catalyst, negative mode

MS studies might also reveal important information, and should always be run.[36] Accordingly, we report both positive and negative MS results.

In the case of **3** + 3,5-DTBC, and in the negative mode, the main ionization product was $[V(3,5\text{-DTBC})_3]^-$ at m/z = 711.3884 (calcd. m/z = 711.3835). Other species in the negative mode are $[VO(3,5\text{-DTBC})_2]^-$ at m/z = 507.2336 (calcd. m/z = 507.2321). A very low-intensity signal can be observed for $[VO(HL^{Saltris})(3,5\text{-DTBC})]^-$ at m/z = 622.2976 (calcd. m/z = 622.2954). In the positive mode the only clearly detected species is [3,5-DTBQ + Na]$^+$ at m/z = 243.1400 (calcd. m/z = 243.1356). However, there exists a very low-intensity (*ca.* 2 %) signal at m/z = 646.2889. We have tentatively assigned this to the species $[VO(H_2L^{Saltris})(O\text{-}3,5\text{-DTBC}) + Na]^+$, which has a calculated m/z = 646.2919. There are no traces of the intact **3** in either positive or negative polarization. From this data, the detection of $[VO(3,5\text{-DTBC})_2]^-$ or, perhaps $[V(IV)O(3,5\text{-DTBC})(3,5\text{-DTBSQ})]^-$, is significant, as it has been linked to the Pierpont's complex $[V(V)O(3,5\text{-DTBC})(3,5\text{-DTBSQ})]_2$, which is the dimerized resting state of the supposed active catalyst [VO(3,5-DTBC)(3,5-DTBSQ)].[38] Pierpont's complex, having a calculated m/z = 1014.4631, is not detected, however. The MS spectra are presented in the ESI (figures S42–43).

With **3** + 4-TBC, a somewhat similar speciation is observed, however, the main species in the negative ionization corresponds to $[VO(HL^{Saltris})(O\text{-}4\text{-TBC})]^-$ at m/z = 566.2312 (calcd. m/z = 566.2328). The tris catecholato species $[V(4\text{-TBC})_3]^-$ is also present at m/z = 543.1966 (calcd. m/z = 543.1957) with low intensity. These findings may suggest that in the presence of 4-TBC, which reacts slower than 3,5-DTBC, **3** is somewhat more inclined to form monocatecholato adducts. This would also give some credibility to the ^{51}V NMR assignment at –438 ppm (see above). Similarly to the above case, the $[VO(H_2L^{Saltris})(O\text{-}4\text{-TBC}) + Na]^+$ low-intensity adduct is tentatively assigned to the m/z = 590.2240 observed in the positive mode (calcd. m/z = 590.2293). [**3** + Na]$^+$ is also detected in the positive ionization mode with m/z = 825.2625 (calcd. m/z = 825.2706) unlike previously in the presence of 3,5-DTBC. The MS spectra are presented in the ESI (figures S44–S45).

After overnight reaction of 3,5-DTBC in the presence of 1 mol-% **3** three compounds were isolated (table 5 and ESI). The product distribution resembles that found in many 3,5-DTBC oxidation reactions catalyzed by a variety of different vanadium pre-catalysts.[35,36,38] For instance, the 7-membered 3,5-di-*tert*-butyl-1-oxacyclohepta-3,5-diene-2,7-dione (**4**) is generally obtained with the highest yield of 40–57 % of the reaction products. While our isolated yield falls slightly short of 40 %, it is still the main product at 31 % yield. The second to most abundant product is 3,5-di-*tert*-butyl-1,2-benzoquinone (**5**) with a mean yield of 9–25 % and agrees with our observations (yield = 23 %). Additionally, the dimeric 4',6,6',8-tetra-*tert*-butyl-*3H*-spiro[benzo[*b*][1,4]di-oxine-2,2'-pyran]-3-one (**6**) represents one of the low-yielding products (10–18 %), a fact which is also observed by us (18 % yield). However, we were unable to isolate, nor detect, the lactones 3,5-di-*tert*-butyl-2-pyrone (**7**) or 3,5-di-*tert*-butyl-5-(carboxymethyl)-2-furanone (**8**) which generally, and in combination, represent at most 20 % of the total

product yield. Accordingly, they might represent the "missing" 28 %, as the combined *isolated* yield of our reaction amounts to only 72 %. TLC was however used to establish that no 3,5-DTBC was present, and hence we estimate a minimum 95 % conversion. It is important to emphasize that the formation of the products **4**, **6**, **7** and **8**, which represent the dioxygenase intra- and extradiol cleavage products, have been linked[36,38] to the vanadium species $[V(3,5\text{-DTBC})_3]^-$ (detected with ESI-HRMS, see above), which is itself intimately related to [VO(3,5-DTBC)(3,5-DTBSQ)] and the "common catalyst hypothesis".[36]

Table 5. The product distribution obtained by reacting 3,5-DTBC with air in boiling chloroform in the presence of 1 mol-% **3**.

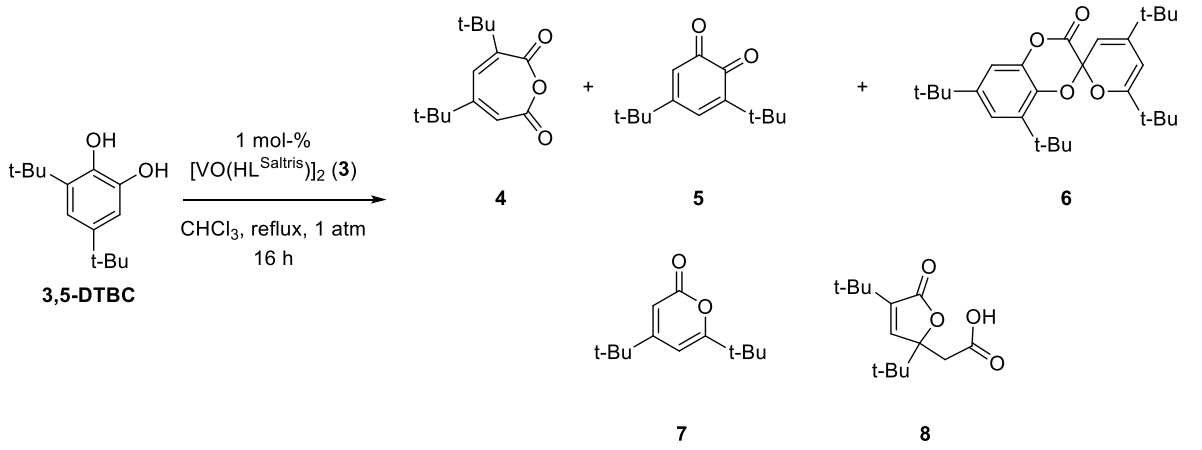

	Isolated product yield (%)				
Estimated conversion[a] (%)	**4**	**5**	**6**	**7**	**8**
≥95	31	23	18	nd[b]	nd[b]

[a] As determined by TLC. [b] Not detected. Reaction conditions: 500 mg 3,5-DTBC, 18 mg **3**, 30 mL $CHCl_3$, reflux 16 h.

The mechanistic investigations described above provide compelling evidence in support of the notion that neither **3**, nor a close structural derivative thereof, is the active catechol oxidation catalyst. Consequently, a catalytic cycle resembling the one described for the closely similar dicobalt system cannot be credibly proposed.[28] Instead, the results obtained from UV-Vis, ^{51}V NMR, and from the ESI-HRMS and product distribution experiments in particular, confer a rather different state of affairs. The combined results clearly indicate that dioxygenase activity is presented during catalysis as well, and that the system presented herein confers very similar behavior to many other vanadium precatalysts. These results are decisively in favor of the "common catalyst hypothesis".[36]

Oxygen atom transfer activity

cis-Dioxidomolybdenum(VI) and –tungsten(VI) complexes are well known to catalyze oxygen atom transfer (OAT) to suitable organic substrates such as, but not limited to, benzoin and triphenylphosphine.[82–86] The propensity of Mo/W compounds to catalyze this particular reaction is not at all surprising considering the role of these metals in enzymes such as DMSO reductase that catalyzes similar reactions.[86] As a

result, oxidovanadium complexes have generally received much less attention in this regard. We chose tris(4-fluorophenyl)phosphine as the model compound, due to the ease of monitoring of the reaction by the very sensitive and quantitative ^{19}F NMR.[55] Quite unexpectedly, however, the complexes were found to not have any significant OAT activity, even at moderate catalyst loadings of 10 mol-% (ESI figure S58).

Conclusions

Mononuclear complexes $[MO_2(H_2L^{Saltris})]$ (M = Mo (**1**), W (**2**)), as well as a dinuclear complex $[VO(HL^{Saltris})]_2$ (**3**) with a hydroxyl-rich Schiff base proligand *N*-(1,3-dihydroxy-2-(hydroxymethyl)propan-2-yl)-3,5-di-*tert*-butylsalicylaldimine ($H_4L^{Saltris}$), were prepared by the reaction with Mo, W and V metal precursors in methanol solutions. The dinuclear vanadium complex shows moderate activity in the oxidation of 4-TBC and 3,5-DTBC, mimicking the action of the dicopper enzyme catechol oxidase. Strikingly, the activity of **3** in catechol oxidation was observed to be similar to that of a structurally very similar dicobalt complex $[Co(H_2L^{Saltris})(OAc)]_2$, whose mechanism of catalysis has been established. However, a set of experiments investigating the catechol oxidation mechanism by **3**, prompted by similarity to $[Co(H_2L^{Saltris})(OAc)]_2$, strongly hint that **3** is not the catalytically active species in the solution. Rather, the presented mechanistic studies reinforce a strong argument in the literature which suggests that a catecholato-bearing vanadium species is formed *in-situ* during catalytic turnover conditions in the presence of 3,5-DTBC, is in fact the real active catalyst. It is further proposed, that such a complex is formed in virtually every scenario involving vanadium-based precatalysts and 3,5-DTBC, a fact clearly demonstrated by the $[VO(HL^{Saltris})]_2$ system presented herein. Furthermore, and quite unexpectedly, the complexes were revealed not to demonstrate any significant OAT activity in the oxidation of ($P(p\text{-}C_6H_4F)_3$), even when moderate catalyst loadings were employed.

Conflicts of interest

The authors declare no competing interests.

Electronic Supplementary Information

All spectra relevant to the characterization of the compounds are presented in the ESI, as well as detailed descriptions of the syntheses.

Acknowledgements

Dr. Milla Suominen is greatly acknowledged for assisting in electrochemistry measurements. Dr. Isabella Norrbo, Hannah Byron and Sami Vuori are accredited for performing the powder XRD measurements. University of Jyväskylä is kindly thanked for the access to their XRD facilities. AP gratefully acknowledges the Academy of Finland for funding (grant no. 315911). PS greatly acknowledges the University of Turku Graduate School (UTUGS) Doctoral Programme in Physical and Chemical Sciences (PCS) for funding.

References

[1] C.L. Hill, I.A. Weinstock, On the trail of dioxygen activation, Nature. 388 (1997) 332–333. doi:10.1038/40986.

[2] J. Ibers, R. Holm, Modeling coordination sites in metallobiomolecules, Science (80-.). 209 (1980) 223–235. doi:10.1126/science.7384796.

[3] K. Karlin, Metalloenzymes, structural motifs, and inorganic models, Science (80-.). 261 (1993) 701–708. doi:10.1126/science.7688141.

[4] R. Hille, The molybdenum oxotransferases and related enzymes, Dalt. Trans. 42 (2013) 3029–3042. doi:10.1039/c2dt32376a.

[5] R. Hille, T. Nishino, F. Bittner, Molybdenum enzymes in higher organisms, Coord. Chem. Rev. 255 (2011) 1179–1205. doi:10.1016/j.ccr.2010.11.034.

[6] R. Hille, The Mononuclear Molybdenum Enzymes, Chem. Rev. 96 (1996) 2757–2816. doi:10.1021/cr950061t.

[7] C. Schulzke, Molybdenum and Tungsten Oxidoreductase Models, in: Bioinspired Catal., Wiley-VCH Verlag GmbH & Co. KGaA, Weinheim, Germany, 2014: pp. 349–382. doi:10.1002/9783527664160.ch13.

[8] D.C. Crans, J.J. Smee, E. Gaidamauskas, L. Yang, The chemistry and biochemistry of vanadium and the biological activities exerted by vanadium compounds, Chem. Rev. 104 (2004) 849–902. doi:10.1021/cr020607t.

[9] M. Kirihara, Aerobic oxidation of organic compounds catalyzed by vanadium compounds, Coord. Chem. Rev. 255 (2011) 2281–2302. doi:10.1016/j.ccr.2011.04.001.

[10] C. Bolm, Vanadium-catalyzed asymmetric oxidations, Coord. Chem. Rev. 237 (2003) 245–256. doi:10.1016/S0010-8545(02)00249-7.

[11] R.R. Langeslay, D.M. Kaphan, C.L. Marshall, P.C. Stair, A.P. Sattelberger, M. Delferro, Catalytic Applications of Vanadium: A Mechanistic Perspective, Chem. Rev. 119 (2019) 2128–2191. doi:10.1021/acs.chemrev.8b00245.

[12] D. Rehder, J. Costa Pessoa, C.F.G.C. Geraldes, M.M. Castro, T. Kabanos, T. Kiss, B. Meier, G. Micera, L. Pettersson, M. Rangel, A. Salifoglou, I. Turel, D. Wang, In vitro study of the insulin-mimetic behaviour of vanadium(IV, V) coordination compounds, JBIC J. Biol. Inorg. Chem. 7 (2002) 384–396. doi:10.1007/s00775-001-0311-5.

[13] D. Rehder, The role of vanadium in biology, Metallomics. 7 (2015) 730–742. doi:10.1039/C4MT00304G.

[14] D. Rehder, The potentiality of vanadium in medicinal applications, Future Med. Chem. 4 (2012) 1823–1837. doi:10.4155/fmc.12.103.

[15] T. Klabunde, C. Eicken, J.C. Sacchettini, B. Krebs, Crystal structure of a plant catechol oxidase containing a dicopper center, Nat. Struct. Biol. 5 (1998) 1084–1090. doi:10.1038/4193.

[16] C. Gerdemann, C. Eicken, B. Krebs, The crystal structure of catechol oxidase: New insight into the function of type-3 copper proteins, Acc. Chem. Res. 35 (2002) 183–191. doi:10.1021/ar990019a.

[17] E. Solem, F. Tuczek, H. Decker, Tyrosinase versus catechol oxidase: One asparagine makes the difference, Angew. Chemie Int. Ed. 55 (2016) 2884–2888. doi:10.1002/anie.201508534.

[18] A.A. El-Taras, I.M. EL-Mehasseb, A.E.-M.M. Ramadan, Synthesis, characterization, magnetic, thermal and electrochemical studies of oxidovanadium (IV) picolyl hydrazones as functional catechol oxidase models, Comptes Rendus Chim. 15 (2012) 298–310. doi:10.1016/j.crci.2011.11.009.

[19] M.R. Maurya, B. Uprety, F. Avecilla, P. Adão, J. Costa Pessoa, Vanadium(V) complexes of a tripodal ligand, their characterisation and biological implications, Dalt. Trans. 44 (2015) 17736–17755. doi:10.1039/C5DT02716K.

[20] S.K. Mal, M. Mitra, H.R. Yadav, C.S. Purohit, A.R. Choudhury, R. Ghosh, Synthesis, crystal structure and catecholase activity of a vanadium(V) Schiff base complex, Polyhedron. 111 (2016) 118–122. doi:10.1016/j.poly.2016.03.033.

[21] P. Salonen, A. Peuronen, A. Lehtonen, Oxidovanadium(V) amine bisphenolates as epoxidation, sulfoxidation and catechol oxidation catalysts, Inorg. Chem. Commun. 86 (2017) 165–167. doi:10.1016/j.inoche.2017.10.017.

[22] M.R. Maurya, B. Uprety, F. Avecilla, P. Adão, M.L. Kuznetsov, J. Costa Pessoa, Solution behaviour and catalytic potential towards oxidation of dopamine by oxidovanadium(V) complexes of tripodal tetradentate ligands, Eur. J. Inorg. Chem. 2017 (2017) 3087–3099. doi:10.1002/ejic.201700342.

[23] C. Balakrishnan, M.A. Neelakantan, Crystal structure and bio-catalytic potential of oxovanadium(IV) Schiff base complexes derived from 2-hydroxy-4-(prop-2-yn-1-yloxy)benzaldehyde and alicyclic/aromatic diamines, Inorganica Chim. Acta. 469 (2018) 503–514. doi:10.1016/j.ica.2017.09.060.

[24] M. Rolff, J. Schottenheim, H. Decker, F. Tuczek, Copper–O2 reactivity of tyrosinase models towards external monophenolic substrates: molecular mechanism and comparison with the enzyme, Chem. Soc. Rev. 40 (2011) 4077. doi:10.1039/c0cs00202j.

[25] I.A. Koval, P. Gamez, C. Belle, K. Selmeczi, J. Reedijk, Synthetic models of the active site of catechol oxidase: mechanistic studies, Chem. Soc. Rev. 35 (2006) 814. doi:10.1039/b516250p.

[26] S.K. Dey, A. Mukherjee, Catechol oxidase and phenoxazinone synthase: Biomimetic functional models and mechanistic studies, Coord. Chem. Rev. 310 (2016) 80–115. doi:10.1016/j.ccr.2015.11.002.

[27] M. Mitra, A.K. Maji, B.K. Ghosh, P. Raghavaiah, J. Ribas, R. Ghosh, Catecholase activity of a structurally characterized dinuclear iron(III) complex [FeIII2(L)2] [H3L=N,N′-bis(3-methoxysalicylaldimine)-1,3-diaminopropan-2-ol], Polyhedron. 67 (2014) 19–26. doi:10.1016/j.poly.2013.08.064.

[28] S.K. Dey, A. Mukherjee, The synthesis, characterization and catecholase activity of dinuclear cobalt(II/III) complexes of an O-donor rich Schiff base ligand, New J. Chem. 38 (2014) 4985–4995. doi:10.1039/C4NJ00715H.

[29] M.E. Cass, D.L. Green, R.M. Buchanan, C.G. Pierpont, Orthoquinone complexes of vanadium and their reactions with molecular oxygen, J. Am. Chem. Soc. 105 (1983) 2680–2686. doi:10.1021/ja00347a027.

[30] C.L. Simpson, C.G. Pierpont, Complexes of vanadium(III) and vanadium(IV) containing bipyridine and tetrachlorocatecholate ligands. Insights into the tunicate vanadium(III) coordination environment, Inorg. Chem. 31 (1992) 4308–4313. doi:10.1021/ic00047a018.

[31] S.R. Cooper, Y.B. Koh, K.N. Raymond, Synthetic, structural, and physical studies of bis(triethylammonium) tris(catecholato)vanadate(IV), potassium bis(catecholato)oxovanadate(IV), and potassium tris(catecholato)vanadate (III), J. Am. Chem. Soc. 104 (1982) 5092–5102. doi:10.1021/ja00383a016.

[32] M.E. Cass, N.R. Gordon, C.G. Pierpont, Catecholate and semiquinone complexes of vanadium. Factors that direct charge distribution in metal-quinone complexes, Inorg. Chem. 25 (1986) 3962–3967. doi:10.1021/ic00242a027.

[33] C.R. Cornman, G.J. Colpas, J.D. Hoeschele, J. Kampf, V.L. Pecoraro, Implications for the spectroscopic assignment of vanadium biomolecules: Structural and spectroscopic characterization of monooxovanadium(V) complexes containing catecholate and hydroximate based noninnocent ligands, J. Am. Chem. Soc. 114 (1992) 9925–9933. doi:10.1021/ja00051a026.

[34] J.P. Wilshire, L. Leon, P. Bosserman, D.T. Sawyer, Electrochemical and spectroscopic studies of molybdenum-catechol momplexes: Models for molybdoenzymes and biological transport, in: Molybdenum Chem. Biol. Significance, Springer US, Boston, MA, 1980: pp. 327–344. doi:10.1007/978-1-4615-9149-8_26.

[35] H. Weiner, R.G. Finke, An all-inorganic, polyoxometalate-based catechol dioxygenase that exhibits > 100 000 catalytic turnovers, J. Am. Chem. Soc. 121 (1999) 9831–9842. doi:10.1021/ja991503b.

[36] C.-X. Yin, R.G. Finke, Vanadium-based, extended catalytic lifetime catechol dioxygenases: Evidence for a common catalyst, J. Am. Chem. Soc. 127 (2005) 9003–9013. doi:10.1021/ja051594e.

[37] C.X. Yin, R.G. Finke, Kinetic and mechanistic studies of vanadium-based, extended catalytic lifetime catechol dioxygenases, J. Am. Chem. Soc. 127 (2005) 13988–13996. doi:10.1021/ja052998+.

[38] C.-X. Yin, Y. Sasaki, R.G. Finke, Autoxidation-product-initiated dioxygenases: Vanadium-based, record catalytic lifetime catechol dioxygenase catalysis, Inorg. Chem. 44 (2005) 8521–8530. doi:10.1021/ic050717t.

[39] N. Zwettler, J.A. Schachner, F. Belaj, N.C. Mösch-Zanetti, Hydrogen bond donor functionalized dioxido-molybdenum(VI) complexes as robust and highly efficient precatalysts for alkene epoxidation, Mol. Catal. 443 (2017) 209–219.

doi:10.1016/j.mcat.2017.09.036.

[40] M.K. Hossain, J.A. Schachner, M. Haukka, N.C. Mösch-Zanetti, E. Nordlander, A. Lehtonen, Catalytic epoxidation using dioxidomolybdenum(VI) complexes with tridentate aminoalcohol phenol ligands, Inorganica Chim. Acta. 486 (2019) 17–25. doi:10.1016/j.ica.2018.10.012.

[41] G.J.J. Chen, J.W. McDonald, W.E. Newton, Synthesis of molybdenum(IV) and molybdenum(V) complexes using oxo abstraction by phosphines. Mechanistic implications, Inorg. Chem. 15 (1976) 2612–2615. doi:10.1021/ic50165a008.

[42] F.A. Schröder, J. Scherle, Über die reaktionen von MoO3 und WO3 mit mehrwertigen alkoholen, Zeitschrift Für Naturforsch. B. 28 (1973) 46–55. doi:10.1515/znb-1973-1-213.

[43] G.R. Fulmer, A.J.M. Miller, N.H. Sherden, H.E. Gottlieb, A. Nudelman, B.M. Stoltz, J.E. Bercaw, K.I. Goldberg, NMR Chemical Shifts of Trace Impurities: Common Laboratory Solvents, Organics, and Gases in Deuterated Solvents Relevant to the Organometallic Chemist, Organometallics. 29 (2010) 2176–2179. doi:10.1021/om100106e.

[44] R.K. Harris, E.D. Becker, S.M. Cabral de Menezes, R. Goodfellow, P. Granger, NMR nomenclature: nuclear spin properties and conventions for chemical shifts. IUPAC Recommendations 2001. International Union of Pure and Applied Chemistry. Physical Chemistry Division. Commission on Molecular Structure and Spectroscopy, Magn. Reson. Chem. 40 (2002) 489–505. doi:10.1002/mrc.1042.

[45] A. Lehtonen, M. Wasberg, R. Sillanpää, Dioxomolybdenum(VI) and -tungsten(VI) complexes with tetradentate aminobis(phenol)s, Polyhedron. 25 (2006) 767–775. doi:10.1016/j.poly.2005.07.037.

[46] Y.-L. Wong, L.H. Tong, J.R. Dilworth, D.K.P. Ng, H.K. Lee, New dioxo–molybdenum(vi) and –tungsten(vi) complexes with N-capped tripodal N2O2 tetradentate ligands: Synthesis, structures and catalytic activities towards olefin epoxidation, Dalt. Trans. 39 (2010) 4602–4611. doi:10.1039/b926864b.

[47] A. Peuronen, R. Sillanpää, A. Lehtonen, The syntheses and vibrational spectra of 16O- and 18O-enriched cis-MO2 (M=Mo, W) complexes, ChemistrySelect. 3 (2018) 3814–3818. doi:10.1002/slct.201800671.

[48] W.P. Griffith, Transition metal oxo complexes, Coord. Chem. Rev. 5 (1970) 459–517. doi:10.1016/S0010-8545(00)80101-0.

[49] G. Asgedom, A. Sreedhara, J. Kivikoski, J. Valkonen, E. Kolehmainen, C.P. Rao, Alkoxo bound monooxo- and dioxovanadium(V) complexes: Synthesis, characterization, X-ray crystal structures, and solution reactivity studies, Inorg. Chem. 35 (1996) 5674–5683. doi:10.1021/ic960061r.

[50] M.K. Hossain, M. Haukka, G.C. Lisensky, A. Lehtonen, E. Nordlander, Oxovanadium(V) complexes with tripodal bisphenolate and monophenolate ligands: Syntheses, structures and catalytic activities, Inorganica Chim. Acta. 487 (2019) 112–119. doi:10.1016/j.ica.2018.11.049.

[51] CrysAlisPRO, Rigaku Oxford Diffraction, (2015).

[52] G.M. Sheldrick, A short history of SHELX, Acta Crystallogr. Sect. A Found. Crystallogr. 64 (2008) 112–122. doi:10.1107/S0108767307043930.

[53] G.M. Sheldrick, Crystal structure refinement with SHELXL, Acta Crystallogr. Sect. C Struct. Chem. 71 (2015) 3–8. doi:10.1107/S2053229614024218.

[54] R.R. Gagne, C.A. Koval, G.C. Lisensky, Ferrocene as an Internal Standard for Electrochemical Measurements, Inorg. Chem. 19 (1980) 2854–2855. doi:10.1021/ic50211a080.

[55] K. Most, J. Hoßbach, D. Vidović, J. Magull, N.C. Mösch-Zanetti, Oxygen-Transfer Reactions of Molybdenum- and Tungstendioxo Complexes Containing η 2 - Pyrazolate Ligands, Adv. Synth. Catal. 347 (2005) 463–472. doi:10.1002/adsc.200404265.

[56] L.M. Rzepecki, J.H. Waite, A chromogenic assay for catecholoxidases based on the addition of L-proline to quinones, Anal. Biochem. 179 (1989) 375–381. doi:10.1016/0003-2697(89)90148-6.

[57] W. Flaig, T. Ploetz, A. Küllmer, Über ultraviolettspektren einiger benzochinone, Zeitschrift Für Naturforsch. B. 10 (1955) 668–676. doi:10.1515/znb-1955-1202.

[58] Y. Sui, X. Zeng, X. Fang, X. Fu, Y. Xiao, L. Chen, M. Li, S. Cheng, Syntheses, structure, redox and catalytic epoxidation properties of dioxomolybdenum(VI) complexes with Schiff base ligands derived from tris(hydroxymethyl)amino methane, J. Mol. Catal. A Chem. 270 (2007) 61–67. doi:10.1016/j.molcata.2007.01.032.

[59] G. Asgedom, A. Sreedhara, C.P. Rao, Oxovanadium(V) schiff base complexes of trishydroxymethylaminomethane with salicylaldehyde and its derivatives: Synthesis, characterization and redox reactivity, Polyhedron. 14 (1995) 1873–1879. doi:10.1016/0277-5387(94)00461-M.

[60] V.S. Sergienko, V.L. Abramenko, A. V. Churakov, Y.N. Mikhailov, M.D. Surazhskaya, Synthesis and crystal and molecular structure of the [MoO2(L)(H2O)] · H2O complex (L 2– is the anion of 2-[N-(hydroxynaphtylidene)amino]propan-1,2,3-triol), Crystallogr. Reports. 59 (2014) 523–526. doi:10.1134/S106377451404018X.

[61] G.A. Kolawole, K.S. Patel, The stereochemistry of oxovanadium(IV) complexes derived from salicylaldehyde and polymethylenediamines, J. Chem. Soc. Dalt. Trans. (1981) 1241–1245. doi:10.1039/dt9810001241.

[62] L.J. Willis, T.M. Loehr, K.F. Miller, A.E. Bruce, E.I. Stiefel, Raman and infrared spectroscopic studies of dioxomolybdenum(VI) complexes with cysteamine chelates, Inorg. Chem. 25 (1986) 4289–4293. doi:10.1021/ic00243a045.

[63] V.I. Minkin, A. V. Tsukanov, A.D. Dubonosov, V.A. Bren, Tautomeric Schiff bases: Iono-, solvato-, thermo- and photochromism, J. Mol. Struct. 998 (2011) 179–191. doi:10.1016/j.molstruc.2011.05.029.

[64] Z. Rozwadowski, E. Majewski, T. Dziembowska, P. Erik Hansen, Deuterium isotope

effects on 13C chemical shifts of intramolecularly hydrogen-bonded Schiff bases, J. Chem. Soc. Perkin Trans. 2. (1999) 2809–2817. doi:10.1039/a903200b.

[65] R.M. Claramunt, C. López, M.D. Santa María, D. Sanz, J. Elguero, The use of NMR spectroscopy to study tautomerism, Prog. Nucl. Magn. Reson. Spectrosc. 49 (2006) 169–206. doi:10.1016/j.pnmrs.2006.07.001.

[66] C.P. Rao, A. Sreedhara, P.V. Rao, M.B. Verghese, K. Rissanen, E. Kolehmainen, N.K. Lokanath, M.A. Sridhar, J.S. Prasad, Syntheses, structure, reactivity and species recognition studies of oxo-vanadium(V) and -molybdenum(VI) complexes, J. Chem. Soc. Dalt. Trans. (1998) 2383–2394. doi:10.1039/a801226a.

[67] V.L. Abramenko, A. V Churakov, V.S. Sergienko, Y.N. Mikhailov, M.D. Surazhskaya, Inner complex compounds of dioxomolybdenum(VI) with o-oxyazomethines, derivatives of substituted salicylaldehydes and tris(hydroxymethyl)aminomethane. crystal structures of two complexes [MoO(L)] · CH3OH; L = Z-substituted salicylalimines, Z = 3-NO2 and 3, Russ. J. Coord. Chem. 39 (2013) 553–559. doi:10.1134/S1070328413080010.

[68] D. Rehder, C. Weidemann, A. Duch, W. Priebsch, Vanadium-51 shielding in vanadium(V) complexes: A reference scale for vanadium binding sites in biomolecules, Inorg. Chem. 27 (1988) 584–587. doi:10.1021/ic00276a029.

[69] C.R. Groom, I.J. Bruno, M.P. Lightfoot, S.C. Ward, The Cambridge Structural Database, Acta Crystallogr. Sect. B Struct. Sci. Cryst. Eng. Mater. 72 (2016) 171–179. doi:10.1107/S2052520616003954.

[70] Y.-J. Jang, S.-J. Mo, B.-K. Koo, Molybdenum(VI)- and tungsten(VI)- dioxo complexes with Schiff base ligands, Bull. Korean. Chem Sox. 19 (1998) 587–590.

[71] U. Sandbhor, S. Padhye, E. Sinn, Cis di-oxomolybdenum(VI) complexes with a tridentate ONO donor ligand; synthesis, X-ray crystal structure, spectroscopic properties and oxotransfer chemistry, Transit. Met. Chem. 27 (2002) 681–685. doi:10.1023/A:1019839308548.

[72] D.F. Back, C.R. Kopp, G. Manzoni de Oliveira, P.C. Piquini, New oxidovanadium(V) complexes of the cation [VO]3+: Synthesis, structural characterization and DFT studies, Polyhedron. 36 (2012) 21–29. doi:10.1016/j.poly.2012.01.015.

[73] G.S. Pawley, Unit-cell refinement from powder diffraction scans, J. Appl. Crystallogr. 14 (1981) 357–361. doi:10.1107/S0021889881009618.

[74] T. Weyhermüller, T.K. Paine, E. Bothe, E. Bill, P. Chaudhuri, Complexes of an aminebis(phenolate) [O,N,O] donor ligand and EPR studies of isoelectronic, isostructural Cr(III) and Mn(IV) complexes, Inorganica Chim. Acta. 337 (2002) 344–356. doi:10.1016/S0020-1693(02)01000-9.

[75] X.-Q. Zhu, C.-H. Wang, H. Liang, Scales of Oxidation Potentials, pKa , and BDE of Various Hydroquinones and Catechols in DMSO, J. Org. Chem. 75 (2010) 7240–7257. doi:10.1021/jo101455m.

[76] M.J. Sever, J.J. Wilker, Visible absorption spectra of metal–catecholate and metal–tironate complexes, Dalt. Trans. (2004) 1061–1072. doi:10.1039/B315811J.

[77] S. Mukherjee, T. Weyhermüller, E. Bothe, K. Wieghardt, P. Chaudhuri, Dinuclear and mononuclear manganese(IV)-radical complexes and their catalytic catecholase activity, Dalt. Trans. (2004) 3842–3853. doi:10.1039/B410842F.

[78] I.A. Koval, K. Selmeczi, C. Belle, C. Philouze, E. Saint-Aman, I. Gautier-Luneau, A.M. Schuitema, M. van Vliet, P. Gamez, O. Roubeau, M. Lüken, B. Krebs, M. Lutz, A.L. Spek, J.-L. Pierre, J. Reedijk, Catecholase activity of a copper(II) complex with a macrocyclic ligand: Unraveling catalytic mechanisms, Chem. - A Eur. J. 12 (2006) 6138–6150. doi:10.1002/chem.200501600.

[79] J. Ackermann, F. Meyer, E. Kaifer, H. Pritzkow, Tuning the activity of catechol oxidase model complexes by geometric changes of the dicopper core, Chem. - A Eur. J. 8 (2002) 247–258. doi:10.1002/1521-3765(20020104)8:1<247::AID-CHEM247>3.0.CO;2-P.

[80] J. Reim, B. Krebs, Synthesis, structure and catecholase activity study of dinuclear copper(II) complexes, J. Chem. Soc. Dalt. Trans. 0 (1997) 3793–3804. doi:10.1039/a704245k.

[81] I.A. Koval, C. Belle, K. Selmeczi, C. Philouze, E. Saint-Aman, A.M. Schuitema, P. Gamez, J.-L. Pierre, J. Reedijk, Catecholase activity of a μ-hydroxodicopper(II) macrocyclic complex: structures, intermediates and reaction mechanism, JBIC J. Biol. Inorg. Chem. 10 (2005) 739–750. doi:10.1007/s00775-005-0016-2.

[82] H. Arzoumanian, Molybdenum-oxo chemistry in various aspects of oxygen atom transfer processes, Coord. Chem. Rev. 178–180 (1998) 191–202. doi:10.1016/S0010-8545(98)00056-3.

[83] M.R. Maurya, B. Mengesha, B. Uprety, N. Jangra, R. Tomar, F. Avecilla, Oxygen atom transfer between DMSO and benzoin catalyzed by cis -dioxidomolybdenum(VI) complexes of tetradentate Mannich bases, New J. Chem. 42 (2018) 6225–6235. doi:10.1039/C7NJ03551A.

[84] C.J. Whiteoak, G.J.P. Britovsek, V.C. Gibson, A.J.P. White, Electronic effects in oxo transfer reactions catalysed by salan molybdenum(VI) cis-dioxo complexes, Dalt. Trans. 2 (2009) 2337. doi:10.1039/b820754b.

[85] M.K. Hossain, J.A. Schachner, M. Haukka, A. Lehtonen, N.C. Mösch-Zanetti, E. Nordlander, Dioxidomolybdenum(VI) and -tungsten(VI) complexes with tripodal amino bisphenolate ligands as epoxidation and oxo-transfer catalysts, Polyhedron. 134 (2017) 275–281. doi:10.1016/j.poly.2017.04.036.

[86] A. Majumdar, S. Sarkar, Bioinorganic chemistry of molybdenum and tungsten enzymes: A structural–functional modeling approach, Coord. Chem. Rev. 255 (2011) 1039–1054. doi:10.1016/j.ccr.2010.11.027.